THESIS

A COMPREHENSIVE ANALYSIS OF ICE NUCLEATING PARTICLES IN A SUBARCTIC URBAN ENVIRONMENT DURING THE ALPACA CAMPAIGN

Submitted by

Samantha Greeney

Department of Atmospheric Science

In partial fulfillment of the requirements

For the Degree of Master of Science

Colorado State University

Fort Collins, Colorado

Fall 2025

Master's Committee:

Advisor: Sonia Kreidenweis
Co-Advisor: Jessie Creamean

Ellison Carter
Emily Fischer

ABSTRACT

A COMPREHENSIVE ANALYSIS OF ICE NUCLEATING PARTICLES IN A SUBARCTIC URBAN ENVIRONMENT DURING THE ALPACA CAMPAIGN

Ice nucleating particles (INPs) influence cloud properties, precipitation, and radiative forcing, yet their sources and characteristics remain poorly understood, especially in polluted Arctic and subarctic environments. This study investigates the size and composition of immersion-mode INPs during the Alaskan Layered Pollution And Chemical Analysis (ALPACA) field campaign, conducted in Fairbanks, Alaska, from January 17 to February 25, 2022. Fairbanks is a unique location with extremely cold conditions, frequent temperature inversions, and persistent wintertime pollution. We report on INP data from online measurements from a continuous flow diffusion chamber (CFDC) and offline filter and size-resolved impactor samples. Interpretation of the observations was supported by contextual aerosol size and composition data.

Our findings show that while the aerosol population was dominated by smaller particles by both number and mass concentrations, INP activity was concentrated in the larger (1.21-12 μm) size ranges. INPs were primarily composed of heat-labile organic material across all size ranges and freezing temperatures, with over 90% of INPs at -15°C and -20°C identified as proteinaceous or biological in origin. Local sources, such as lichen and road gravel, were likely contributors to the observed INP population. Compared to other urban and Arctic sites, Fairbanks exhibited higher INP concentrations at colder temperatures and lower concentrations at warmer ones. These results provide new insight into subarctic INP sources during poor air

quality and emphasize the importance of particle size and local emissions in determining INP activity and abundance.

ACKNOWLEDGMENTS

I would like to express my sincere gratitude to Drs. Sonia Kreidenweis and Jessie Creamean for their invaluable guidance, mentorship, and support throughout my M.S. journey. I am also thankful to the members of our lab, who were always willing to assist in running samples and thoughtful scientific discussions about data challenges. I am grateful to Dr. William Simpson, the chief scientist for the ALPACA campaign, as well as Drs. Brice Temime-Roussel, Barbara D'Anna, Kathy Law, and Rodney Weber for generously allowing me to use the data they collected during the campaign. Drs. Paul DeMott, Russell Perkins, and Ezra Levin provided tremendous help with operating the CFDC during ALPACA, and Paul's input was very helpful in interpreting the resulting data.

My passion for atmospheric research was first sparked by my undergraduate mentor, Dr. Sarah Brooks, whose encouragement and support set me on the path that led me here. I also had the privilege of working as an undergraduate summer intern under the mentorship of Drs. Paul DeMott, Tom Hill, and Kathryn Moore. Their guidance made that summer not only a valuable learning experience but also an enjoyable one. Finally, I am deeply thankful to my parents, fiancé, family, and friends, who saw potential in me even when I did not see it in myself, and who have always encouraged and supported me to pursue my dreams.

This research was supported by the National Science Foundation (NSF) under grant number AGS-2037119.

TABLE OF CONTENTS

LIST OF FIGURES

1. Introduction

The formation of ice in clouds plays a critical role in cloud microphysics, influencing cloud lifetime, radiative forcing, and precipitation processes (DeMott et al., 2010). Ice nucleating particles (INPs) are a subset of aerosols capable of forming ice crystals at temperatures above -38°C, the homogeneous freezing point of pure water (Pruppacher & Klett, 1997). For temperatures between 0°C and -38°C, certain aerosols can serve as INPs and initiate freezing through various mechanisms. Immersion freezing happens when a supercooled droplet containing a suspended INP freezes; condensation freezing is similar to immersion freezing but occurs when a cloud condensation nucleus (CCN) immediately triggers freezing of water condensate; contact freezing occurs when a supercooled droplet freezes upon contacting an aerosol; and deposition freezing occurs when ice forms directly on an INP in a supersaturated environment (Vali, 1985). While natural sources such as sea spray, mineral dust, and biological aerosols are recognized contributors to INP populations (Conen et al., 2011; DeMott et al., 2018; Hoose & Möhler, 2012; Petters et al., 2009; Kanji et al. 2017; Huang et al. 2021), the role of air pollution as a source of INPs remains uncertain. The World Health Organization (WHO) defines pollution to be contamination either in an indoor or outdoor environment by any chemical, physical, or biological agent that alters the natural characteristics of the atmosphere. We focus on pollution in the form of particulate matter, which is the dominant air quality concern in Fairbanks. Since INPs represent a subset of the total aerosol population, it might be expected that higher aerosol number concentrations, such as those that occur in pollution events, might also lead to enhancements in INP concentrations. However, few studies have directly compared INP concentrations during “clean” and “polluted” episodes in the same location; we review here several of these for which particulate matter was the main component during polluted episodes.

For instance, research in Oliktok Point, Alaska, near the Prudhoe Bay oilfield, demonstrated that local pollution events involving soot and fly ash did not contribute significantly to INP concentrations (Creamean et al., 2018). Two other studies also showed that ship exhaust and diesel engine emissions did not influence INP concentrations (McCluskey et al. 2018 and Schill et al. 2016). In a study in Beijing, anthropogenic dust was identified as a contributor to INPs, but pollution events involving poor air quality did not lead to increased concentrations (Chen et al. 2024). However, another study at Beijing's Cloud Laboratory and Observational Utilities Deployment Base (CLOUD Base) located in a suburban area, found that anthropogenic organic aerosols contributed to INP concentrations active at -30°C (Tian et al. 2022). In Mexico City, INP concentrations remained unchanged between "clean" and "polluted" periods (Cabrera-Segoviano et al., 2022). Similarly, research in New Delhi revealed no substantial differences in INP concentrations during pollution events (Wagh et al., 2021). Since the mix of pollutants and atmospheric boundary conditions are unique to every location, it is important to look at more sites to confirm the role of pollution to INP concentrations. Fairbanks, Alaska is characterized by both high wintertime particulate pollution and boundary conditions that strongly influence pollutant buildup.

There is limited research on size-resolved INP measurements, particularly in urban environments that often experience poor air quality. Understanding the size distribution of INPs can help identify potential sources. For instance, determining the percentage of INPs in the supermicron range can rule out contributions to INPs from particles like black carbon, which are predominantly submicron (Clarke et al., 2004; Schwarz et al., 2008, 2013). Conversely, identifying a high proportion of submicron INPs can eliminate intact larger particles, such as fungal spores, as primary contributors (Graham et al., 2003; Elbert et al., 2007; Sesartic and

Dallafior, 2011; Després et al., 2012; Huffman et al., 2012). Additionally, understanding the size distributions of INPs can be beneficial for parameterizations used in cloud microphysics models. For example, DeMott et al. (2010) estimates INP concentrations at different temperatures using the number concentration of particles with diameters larger than 0.5 μm.

Previous studies have produced mixed findings on the size distribution of INPs. Mason et al. (2016) sampled aerosol at seven locations (five in Canada, one in the USA, and one in France) and found that the majority of INPs (60–90% at -15°C, -20°C, and -25°C) had aerodynamic diameters greater than 1 μm. In contrast, Huffman et al. (2013) conducted a study in Manitou Experimental Forest, Colorado, analyzing INP concentrations during rain and dry periods for particles ranging from 0.32 to 18 μm. Their results showed that during rain periods, there were more immersion and deposition freezing INPs in the supermicron regime (~89%) compared to dry periods (~46%) at temperatures between -15°C and -20°C. They also noted an increase in biological particles during rain periods, which could be a potential source of these supermicron INPs. However, a study in the European territory of the former Soviet Union found that only 37% of condensation-freezing INPs at -15°C to -20°C were in the supermicron size range (Berezinski et al., 1988). In West Plains, Missouri, one study showed that 14% of INPs were larger than 1 μm between -12°C and 25°C (Rucklidge 1965). Another study that took place in the central and western south Pacific Ocean and reported by Rosinski et al. (1986) found that 100% of immersion-freezing INPs at -10.8°C had diameters > 1 μm. While limitations of the experiment couldn't assign the composition of these supermicron particles, they did find for smaller INPs (0.1-0.3 μm) that they were mainly organic. These percentages from Huffman et al. (2013), Berezinski et al., (1988), Rucklidge (1965), and Rosinski et al. (1986), were calculated by Mason et al. (2016) in their Table 2. Lastly, Creamean et al. (2022) conducted a study in the

central Arctic, revealing seasonal variations in the size distribution of INPs. During summer, the highest fraction of INPs was observed in the 1-3 μm size range and was attributed to potential local biological sources, while in spring and autumn, INPs were predominantly in the larger size ranges (>3 μm) and attributed to transported sea spray. In contrast, winter conditions favored relatively high concentrations of smaller INPs (<0.34 μm) from long-range transport.

Overall, field measurements of size-resolved INPs are limited, with conflicting evidence regarding whether most INPs are supermicron-sized and the specific temperatures at which supermicron particles represent major or minor contributions. Some studies suggest that supermicron particles dominate INP populations, while others report that less than 40% of INPs are in the supermicron range, although this relationship can change based on the sources of aerosols, whether in urban versus rural, or polluted versus clean locations.

The Alaskan Layered Pollution And Chemical Analysis (ALPACA) campaign took place in winter 2022 in Fairbanks, Alaska. Fairbanks, a small city with a population of 32,515, is situated in Alaska's interior and surrounded by elevated terrain, which significantly influences the local climate. During winter, Fairbanks frequently experiences temperature inversions due to its valley location, topographic shielding from wind, and cold subarctic conditions (Willis & Grice, 1977). The lack of sunlight during winter months further exacerbates these inversions (Wendler & Jayaweera, 1972). Primary sources of wintertime pollution in Fairbanks include burning of residential fuel oil, which is the dominant source of particulate-phase sulfur (Moon et al. 2023, Wang et al. 2014, Ward et al. 2012, Ye et al. 2020, and Campbell et al. 2022), and wood combustion (Nicholls et al., 2010). Within a 32-square-mile radius of Fairbanks, four coal-fired power plants supply energy and emit metallic pollutants and steam (water vapor) (Brett et al.

2025). The Chena River, flowing through the city, also serves as an additional source of water vapor. The combination of cold temperatures, atmospheric inversions, adequate water vapor, and higher aerosol concentrations frequently results in the formation of ice fog (Schmitt et al. 2013). Under these inversion conditions, which occur approximately 50% of the time between November and March, pollutants become trapped near the surface, leading to poor air quality (Cesler-Maloney et al., 2022; Malingowski et al., 2014; Tran & Mölders, 2011). Lill et al. (2024) demonstrated that INPs in Fairbanks facilitated the formation of an ice fog event during ALPACA and examined INP size distributions before, during, and after the fog, along with associated meteorological conditions and aerosol number concentrations.

We aim to explore these relationships between INP size and composition in the immersion freezing mode, located in a subarctic polluted environment. Our first hypothesis is that particles larger than 1 μm contribute significantly to the INP populations in Fairbanks. Our second hypothesis is that, given the surrounding terrain and frequent inversions that trap pollutants, most INPs in Fairbanks originate from local sources rather than from long-range transport. In order to place INP size and composition into context, we also analyze total aerosol particle size distributions, number and mass concentrations, and aerosol composition during the campaign.

2. Data and Methods

The ALPACA campaign was conducted in Fairbanks, Alaska (64.8401°N, 147.7200°W) from January 17 to February 25, 2022. Measurements presented here were taken at the University of Alaska Fairbanks (UAF) Community Technical College (CTC) at 64.841°N, 147.727°W, 135 m AMSL. During ALPACA, various online and offline instruments were deployed for measurements of INP number concentrations, as well as aerosol number, mass and

compositional measurements. For the offline INP sample collection (including inlet setups) and analysis, and optical particle counter (OPC) measurements, details can be found in Lill et al. (2024) but are briefly described here. Meteorological data were collected as well and are reported in Cesler-Maloney et al. (2022). Instruments were housed either within or outside laboratory containers at CTC. Throughout the 6-week campaign one significant ice fog event coupled with a pollution event occurred between January 29 through February 4, 2022 (Lill et al. 2024).

2.1 INP measurements

2.1.1 Online INP Measurements

The Handix Continuous Flow Diffusion Chamber - Ice Activation Spectrometer (CFDC-IAS) was used to measure INP concentrations in near-real time. This instrument provides an online method for simulating mixed-phase cloud conditions to assess INP activity in aerosols smaller than 2.5 μm. Detailed descriptions of operating and design principles for CFDC can be found in prior literature (Rogers et al. 2001). The CFDC-IAS consists of a temperature- and humidity-controlled chamber with two vertically aligned, ice-coated copper walls maintained at different temperatures to generate a gradient in temperature and water vapor pressure. This configuration creates a region supersaturated with respect to ice. Aerosol particles entering the chamber may nucleate ice directly through deposition freezing or, if appropriate setpoints are chosen to create water supersaturation, can activate as supercooled liquid droplets before freezing via condensation or immersion freezing. After freezing, ice crystals pass through an evaporation zone designed to remove supercooled liquid droplets while preserving the ice phase. Remaining ice crystals are then detected and counted by an optical particle counter at the base of the chamber. The CFDC operates at a sample flow rate of 1.5 L min^{-1}, with response times of

approximately 3-5 minutes. The sample inlet consisted of roughly 3 m of ¼" static dispersive tubing straight up from the CFDC inlet that was insulated outside of the instrument container. Additionally, the inlet included a downward facing funnel at the end to prevent snow from falling in. During ALPACA, the CFDC-IAS was deployed from January 16 to February 25, 2022, and operated at two target temperatures, -30°C and -25°C and detected immersion mode freezing. Sampling occurred at various times throughout each day to capture the temporal variability of INP concentrations.

2.1.2 INP Sample Collection for Offline INP Measurements

Total aerosol samples were collected on polycarbonate filters during the ALPACA campaign. Detailed descriptions of the filters, cleaning procedures, and filter holders are available in Creamean et al. (2024) and Barry et al. (2021a). Ambient air was sampled using a vacuum pump (Thomas oil-less piston compressor/vacuum pump, 2688 series) that operated at an average flow rate of approximately 15 L min^{-1}. Aerosols were collected on 47-mm polycarbonate filters (0.2-µm pore size, backed with a 10-µm polycarbonate filter), housed within pre-sterilized, single-use, open-face Nalgene™ Sterile Analytical Filter Units. Continuous in-line flow rate monitoring was performed using a mass flow meter (TSI 5200-2), and filters were protected from snowfall by a shield.

The Davis Rotating-drum Unit for Monitoring (DRUM; model DA-400 DRUMAir™) was used to collect size-resolved aerosol particles via impaction across four rotating stages. Detailed descriptions of the DRUM setup for INP measurements can be found in Creamean et al. (2018, 2019, and 2022). Each of the four DRUM stages was equipped with sterilized perfluoroalkyl substrate strips coated in a thin layer of petrolatum jelly to capture particles. The nominal aerodynamic diameter size ranges for each stage were as follows: stage A (2.96-12 µm), stage B

(1.12-2.96 μm), stage C (0.34-1.21 μm), and stage D (0.15-0.34 μm). The instrument operated at a flow rate of 27-30 L min^{-1} sampling through a vertical aluminum inlet tube (~1 m long, 4 cm diameter) and was housed in a Pelican™ case measuring 47 × 35.7 × 17.6 cm.

During the ALPACA campaign, filter and DRUM samples were collected over 24-hour periods from January 17-28, 2022, and February 5-21, 2022. During an ice fog event which occurred from January 29-February 4, 2022, sampling frequency increased to 12-hour intervals to capture higher temporal resolution data. After collection, filters were stored at -20°C until analysis, which occurred 4-15 months post-collection at Colorado State University (CSU). DRUM samples were also stored at -20°C and remained frozen until analysis, which occurred approximately 27-29 months post-collection.

2.1.3 Offline INP Sample Analysis

All filters and DRUM samples were processed using the CSU Ice Spectrometer (IS). Detailed methods for the IS can be found in Barry et al. (2021a), Hill et al., (2016), and Creamean et al., (2024). Each filter sample was placed in a 50 mL sterile polypropylene tube containing 8 mL of 0.1-μm-filtered deionized water and shaken at 200 rpm for 20 minutes to resuspend particles. The resulting suspension was diluted in an 11-fold series and pipetted into the IS array, which comprises two 96-well temperature-controlled aluminum blocks fitted with disposable, clean PCR (Polymerase Chain Reaction) wells. In each well, 50 μL of the sample was pipetted, alongside designated wells for deionized water blanks. The trays were placed into the IS, covered with a plexiglass window, and subjected to a controlled temperature decrease of 0.33 °C per minute down to approximately -30 °C.

Select DRUM samples, from approximately every 4 days between January 17 and February 20, 2022, were analyzed for this study. The operating procedure was the same as for the filter samples, but the preparation differed. For DRUM samples, each substrate was placed in a 15 mL sterile polypropylene tube containing 5 mL of 0.1 μm-filtered deionized water. The samples were ultrasonicated for 30 seconds and vortexed at 3,200 rpm for seven 10-second pulses. Each DRUM stage (A-D) was processed separately, with the A and B stages diluted 11-, 121-, 400-, and 8000-fold, while the C and D stages were diluted 11-, 20-, and 400-fold.

Following the initial analysis, a subset of DRUM samples from January 22, February 1, and February 6, 2022, underwent heat and peroxide treatments to further investigate the composition of size-resolved INPs. These dates were selected to represent conditions of near-average, high, and low pollution levels (based on ambient aerosol number and mass concentrations), respectively. Corresponding filter samples also underwent heat and peroxide treatments. For the heat treatments, samples were heated to 95 °C for 20 minutes to denature heat-labile proteins, following methods from Hill et al. (2016), O'Sullivan et al. (2018), and Suski et al. (2018). For the peroxide treatments, 30% H_2O_2 was added to achieve a final concentration of 10%, and the samples were heated to 95 °C for 20 minutes under UV-B illumination to generate hydroxyl radicals. Residual H_2O_2 was subsequently removed using catalase. These peroxide treatments targeted the removal of organic INPs, allowing for the analysis of the remaining inorganic INPs (Suski et al., 2018 and Testa et al. 2021). INP concentrations from both the filters and DRUM samples were calculated following the method of Vali (1971):

$$K(\theta)(L^{-1}) = \frac{ln(1-f)}{V_{drop}} \times \frac{V_{suspension}}{V_{air}},$$

where f is the proportion of droplets frozen, V_{drop} is the volume of each sample in the IS wells, $V_{suspension}$ is the volume used for re-suspension, and V_{air} is the volume of air per sample. The total air volume collected on each filter was determined by the mass flowmeter described above. Uncertainties in the INP concentrations were calculated as 95% binomial confidence intervals, following the approach outlined by Agresti and Coull (1998).

Sample blanks were collected throughout the campaign by briefly exposing unused but cleaned filters to ambient air. These blanks were processed identically to the other samples and used to account for potential contamination from field handling and transportation through sample blank subtraction.

2.1.4 Lichen and Road Gravel INP Sample Analysis

Samples of road gravel and lichen were analyzed to evaluate potential local INP sources during the winter period (Section 3.3.1). Road gravel was collected during the ALPACA campaign, while lichen samples were collected on February 6, 2025, between 11:00 and 15:00 AKST from a location called Creamer's Field (64.84°N, 147.73°W), 2.6 km from the CTC site. Lichen samples were collected directly from both spruce and alder trees, then frozen and shipped to CSU for analysis.

Road gravel samples were sieved through a 250 µm mesh to isolate finer particles, and approximately 0.5 g of material was added to 10 mL of deionized water for resuspension. For lichen samples, the external surfaces were washed by placing the material in a sealable plastic bag with 50 mL of deionized water and ultrasonicated for 30 seconds to dislodge surface particles. Both sample types were processed on the CSU IS using the same method described in

Section 2.1.3, including heat and peroxide treatments to assess the contribution of heat-labile, heat-stable and inorganic INPs.

2.2 Supporting Aerosol Data

2.2.1 Aerosol Size Distributions

Particle number concentrations and size distributions were measured using a commercial OPC (model OPC 1.109, Grimm Aerosol Technik) with a time resolution of 1 minute. The OPC classified individual particles by optical diameter in the range of 0.25-34 μm across 31 size bins, using the intensity of light scattered by particles illuminated by a 655 nm laser diode. Ambient air was sampled 3.5 m above ground level at a flow rate of 1.2 L min^{-1} through a 1.5 m vertical anti-static tube (¼" diameter) that extended outside the shelter roof. To measure particle number concentrations and size distributions below the OPC's detection range, a scanning mobility particle sizer (SMPS; model TSI 3936) was deployed at the CTC site. Ijaz et al. (2024) describe details of the site setup and details of the instrument operations. The SMPS measured particle sizes from 15–660 nm based on electrical mobility diameter. The SMPS operated with a time resolution of 2 minutes.

Particle mass concentrations (μg m^{-3}) were calculated from both instruments, assuming sphericity and a particle density of 1 g cm^{-3}. To create a complete particle size profile spanning 15 nm to 32 μm, SMPS data (15–644 nm) were combined with OPC data (654 nm–32 μm). This cutoff ensured a seamless transition between the SMPS and OPC datasets, accounting for the non-uniform size binning of each instrument. No adjustments to the OPC's standard calibration or size bins were required for merging.

2.2.2 Aerosol Composition

Particle composition measurements were conducted using three different instruments, each designed to capture distinct particle size ranges and compositional information. One of these instruments, the Continuous Particulate Monitor with Energy- Dispersive X-ray Fluorescence (ED-XRF; model Horiba PX-375), measured PM10 (particulate matter with diameters <10μm) mass concentrations and elemental composition. Details on operation and inlet of this instrument can be found in Creamean et al. (2016) and Trebs et al. (2024). The PX-375 operated with a flow rate of 16.7 L min^{-1} and a time resolution of 30 minutes. Particles were collected on a 100 mm diameter Teflon™ PTFE fabric filter tape. X-ray fluorescence (XRF) works by exposing the collected particles to high-energy X-rays, which excite the atoms in the sample and cause them to emit secondary (fluorescent) X-rays. These emitted X-rays have characteristic energies unique to each element, allowing for the identification and quantification of elements. The following elements were detected from the PX-375: titanium (Ti), vanadium (V), chromium (Cr), manganese (Mn), iron (Fe), nickel (Ni), copper (Cu), zinc (Zn), arsenic (As), lead (Pb), aluminum (Al), silicon (Si), sulfur (S), potassium (K), and calcium (Ca) in ng m^{-3}. The instrument was housed in a temperature-controlled enclosure at the CTC site, near the containers that housed the CFDC, filters, DRUM, and other supporting aerosol instruments.

The second instrument used for particle composition was the Particle-Into-Liquid Sampler (PILS) coupled with Ion Chromatography (IC), designed to measure particles within the PM2.5 size range. Campbell et al. (2022) provide details on site setup and sample processing details for a study in Fairbanks in the winter of 2020 and 2021,which was the same as used in ALPACA. Briefly, particles were collected with 47-mm Teflon filters with a gas denuder upstream with a flowrate of 16.7 L min^{-1}. The PILS operates with a time resolution of 23 minutes and quantifies

both cationic and anionic species. In this study, we primarily focused on anionic species, including chloride, nitrate, S(IV), and sulfate, expressed in μg m^{-3}. Anions were measured with a Metrohm 761 (Metrohm USA, Riverside, FL) IC unit with conductivity detection. Cation measurements were only conducted for a few days during the campaign, preventing us from drawing definitive conclusions about them in this paper. The PILS functions by continuously collecting ambient particles and mixing them with a supersaturated water vapor stream, causing the particles to grow into droplets. These droplets are then collected into a liquid sample stream and analyzed for ionic species using techniques such as ion chromatography. This approach enables real-time measurement of major water-soluble aerosol components.

The third instrument employed was the High-Resolution Time-of-Flight Aerosol Mass Spectrometer (HR-ToF-AMS), which measured particle composition in the PM1 size range. Ijaz et al. (2024) further describe the sampling site setup during ALPACA. The HR-ToF-AMS has a time resolution of 2 minutes and quantifies sulfate, nitrate, organics, chloride, and ammonium in μg m^{-3}. The data processing accounts for Composition-Dependent Collection Efficiency (CDCE) to correct for particle bounce effects influenced by the inorganic composition.

3. Results and Discussion

3.1 INP concentrations and size

To examine the relationship between INP concentrations and particle size in Fairbanks, we analyzed data from three INP measurement techniques: the Continuous Flow Diffusion Chamber (CFDC), filter samples, and DRUM impactor samples (Figures 1, 4). Nine sampling periods during the ALPACA campaign (January 18, 22, 27, and February 1 [two periods], 6, 10, 15, and 20, 2022) provided data from all three techniques. Each period lasted 24 hours, except February

1, when filter and DRUM samples were collected over two 12-hour intervals to capture an ice fog event in greater detail (Period A: February 1, 09:00–21:00; Period B: February 1, 21:00–February 2, 09:00).

To further investigate the size dependence of INPs, we estimated size-resolved particle mass concentrations from number size distributions measured by the combined SMPS and OPC, which together spanned 0.015–34 μm (Figure 2). These size distributions were summed over DRUM stages. We also calculated mass concentrations in the 12–34 μm range to capture particles potentially collected on the filters but excluded by the DRUM.

Observed INP concentrations from all three measurement techniques were compared to the DeMott et al. (2010) parameterization, which uses average number concentrations for particles >0.5 μm from the combined SMPS and OPC data (Figures 1, 4). Because the filter and DRUM collected continuously (12 or 24 hours) while the CFDC operated intermittently (Figure 5), average particle number concentrations were calculated separately for the filter/DRUM and CFDC datasets.

We further examined INP size contributions by analyzing each DRUM stage (A–D) individually and calculating the relative percentage contribution to INP concentrations at selected temperatures (Figure 6). Finally, to assess INP size during the high-pollution ice fog event on February 1, we compared that period to other case periods (Figure 7).

3.1.1 INP Instrument Comparison

Given the differences in particle size captured amongst the INP instruments, total aerosol samples collected on filters were compared to the DRUM A–D stage sum (0.15–12 μm) across all common temperatures (Figure 1). In order to evaluate agreement between instruments, we applied

Deming regression to paired measurements from the filter and DRUM A–D sum (Figure 3). In Figure 4, INP concentrations from the CFDC, which has an upper size cut-off of roughly 2.5 µm, were compared to those from the DRUM B–D stage sum (0.15–2.96 µm). Although CFDC data were available at –25 °C and occasionally at –30 °C, DRUM B–D data were more limited at –30 °C, making –25 °C the most consistent basis for inter-instrument comparison.

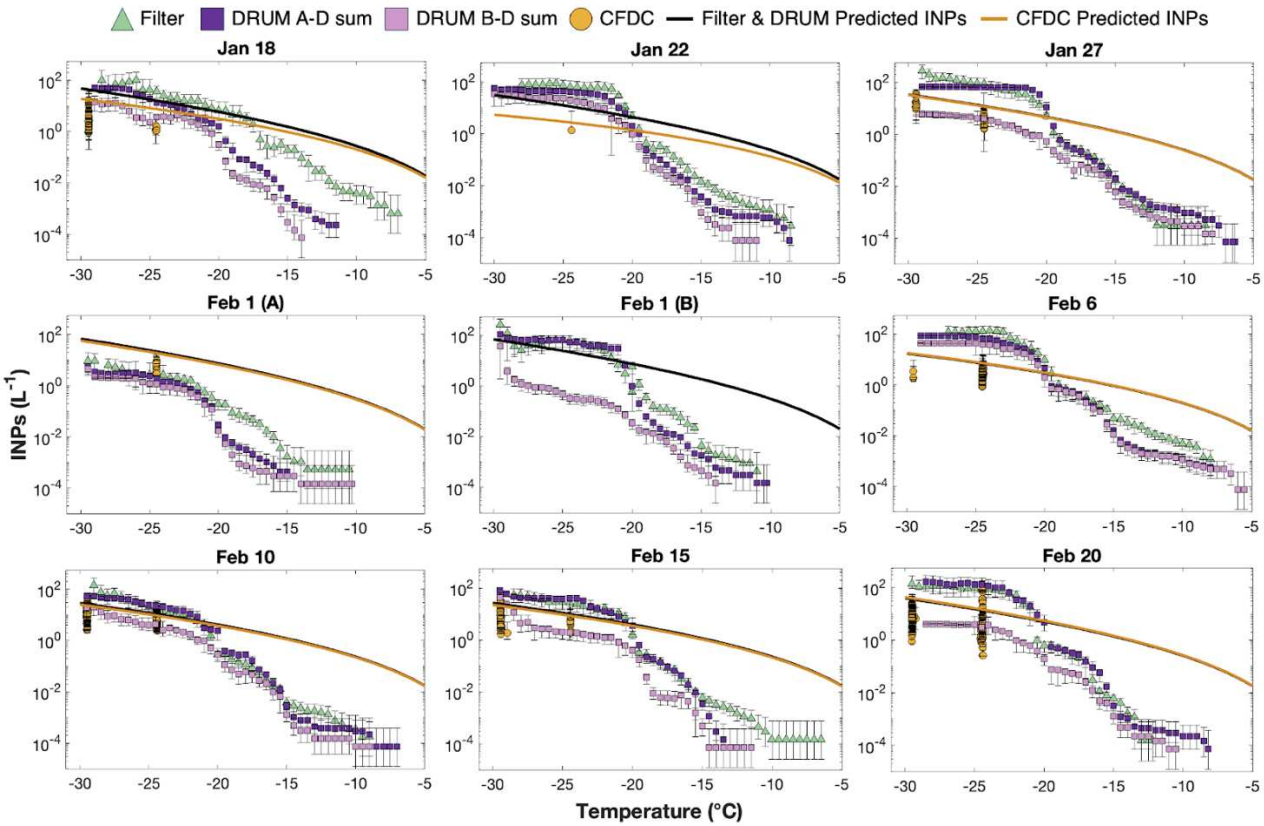

Figure 1. INP concentrations for nine case periods where all three INP measurements yielded data. Green triangles indicate filter-based INP concentrations; dark purple squares show the DRUM A–D stage sum; light purple squares represent the DRUM B–D stage sum; and orange circles represent CFDC data. The lines denote predicted INP concentrations for the filter/DRUM (black) and CFDC (orange) using the DeMott et al. (2010) parameterization.

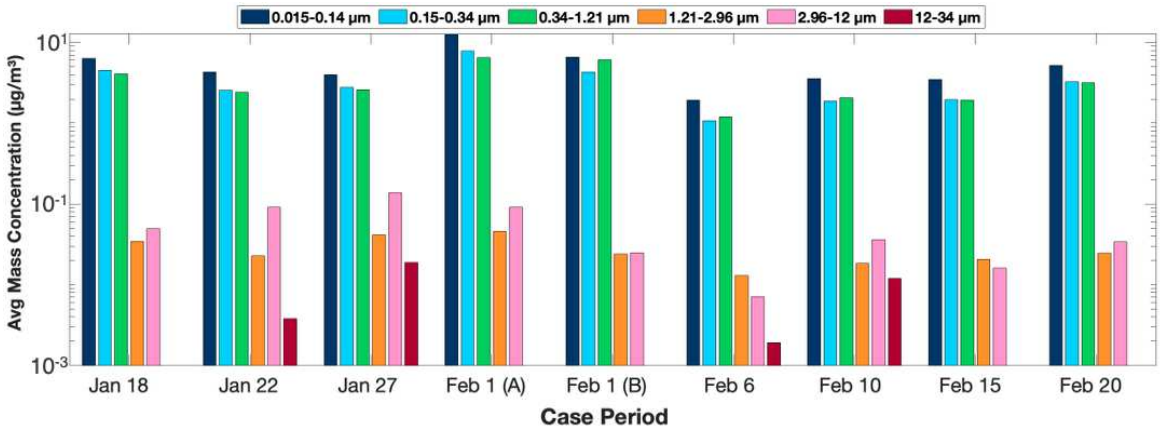

Figure 2. Combined SMPS and OPC data for the average mass concentration of six size ranges, representing the four DRUM stage (A-D) particle size ranges as well as particle sizes below DRUM D and above DRUM A.

Across the full temperature range, filter-based and DRUM A–D sum INP concentrations generally agreed within uncertainty (Figure 1). Agreement was strongest at colder temperatures (–20 °C to –30 °C), where both datasets tended to plateau. In most cases, the steepest increase in INP concentrations occurred between –15 °C and –20 °C, suggesting the presence of a distinct INP population. Warmer temperatures (>–20 °C) showed greater variability between the two techniques, and the magnitude of this variability varied by day.

The largest warm-temperature disagreement occurred on January 18, when filter and DRUM spectra diverged roughly 1.5 to 2 orders of magnitude for temperatures above –20 °C (Figure 1) and exhibited the greatest difference in onset freezing (Filter: –7 °C, DRUM A-D: –11.5 °C). No particle mass was detected in the 12–34 µm size range during this period (Figure 2), suggesting that the difference was not mainly due to the presence of very large particles. However, the OPC likely undercounts particles in the 12–34 µm range due to inlet losses and its lower flow rate, and these size particles are typically very low in concentration in the atmosphere, which collectively makes them difficult to measure. Instances such as January 18, where the filter showed higher concentrations or a much earlier onset freezing temperature could still be explained by its ability

to collect a wider size range, including particles larger than 12 µm. Larger particles are generally more effective INPs (Mason et al., 2016; Creamean et al., 2018, 2019), and the filter's open-faced collection surface (i.e., no inlet) increases the likelihood of capturing them. For all other sampling periods in Figure 1, differences between the filter and DRUM A–D spectra were smaller, remaining within roughly an order of magnitude. Previous intercomparison studies have shown that such variability is within the expected range for offline INP instruments sampling the same air (DeMott et al., 2018; Lacher et al., 2024). Given Fairbanks' aerosol size distribution and the consistent agreement within an order of magnitude, these results suggest that most INPs in Fairbanks are captured within the DRUM A–D size range (0.15–12 µm).

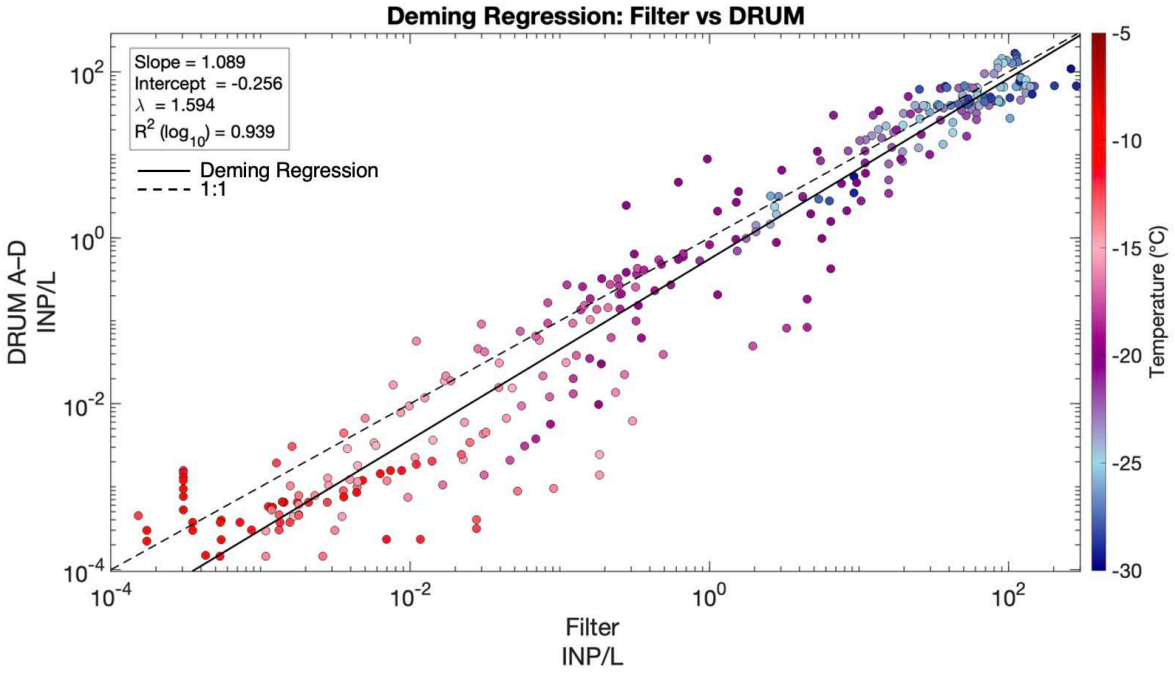

Figure 3. INP concentrations from all nine case periods from the filter (X axis) and DRUM A-D sum (Y axis) with Deming regression (yellow line) and 1:1 (black dashed line)

To further compare the filter and the DRUM A–D sum INP concentrations, we combined data from all nine case study dates into a single Deming regression analysis (Figure 3). This

method accounts for uncertainty in both instruments, rather than assuming only the y-variable has error, and uses the ratio of variances (λ) to balance their relative precision. In our case, λ was greater than one (1.594), which suggests that the DRUM measurements were noisier relative to the filter, and the regression line therefore weighted the filter values more strongly.

The resulting regression had a slope of 1.089 and an intercept of –0.256 (in log space). A slope of 1 would indicate perfect proportionality across the concentration range of both instruments. In our case, a slope slightly greater than 1 indicates that DRUM concentrations increase somewhat more steeply relative to the filter as INP abundance rises. The negative intercept implies that at lower concentrations (warmer activation temperatures), the DRUM tended to report slightly lower values than the filter. These results suggest that while the filter and DRUM A–D track each other closely ($R^2 = 0.939$), the DRUM is generally consistent with the filter across most concentrations, with slight underestimation at the low end and modestly steeper scaling at the high end. This slight disagreement at the warm end of the spectra aligns with the fact that the filter's open-faced collection allows it to capture larger particles, whereas the DRUM can only sample up to 12 µm and may also experience inlet losses.

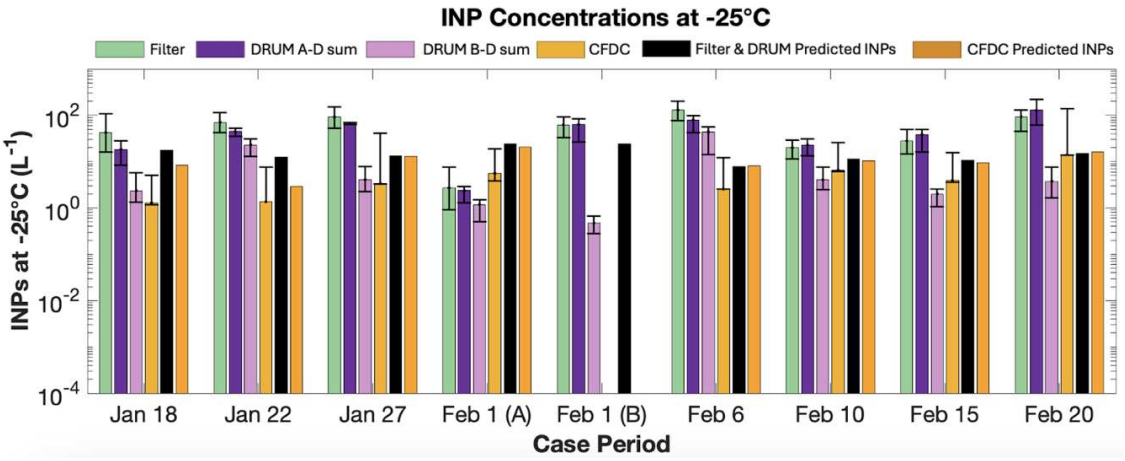

Figure 4. INP concentrations at –25 °C from filter (green), DRUM A–D (dark purple), DRUM B–D (light purple), and CFDC (orange) measurements. Predicted INP concentrations for filter/DRUM (black) and CFDC (dark orange) are shown for comparison.

At –25 °C, filter and DRUM A–D sum concentrations were consistently higher than CFDC and DRUM B–D sum concentrations (Figure 4), as expected from the inclusion of particles >2.5 µm. CFDC and DRUM B–D concentrations at –25 °C agreed within uncertainty for six of the eight available sampling periods. The DRUM operated as an offline technique, continuously collecting particles over a 12- or 24-hour period, whereas the CFDC sampled at discrete times throughout the day. Figure 5 shows a detailed comparison of CFDC sampling times. The largest disagreements occurred when CFDC sampling was limited. For example, on January 22 the CFDC measured roughly 22 INPs L^{-1} fewer than the DRUM B–D sum because it only sampled during a single 5-minute period. On February 6, although the CFDC operated during many more periods, it still measured about 40 INPs L^{-1} fewer than the DRUM, which had continuous 24-hour collection.

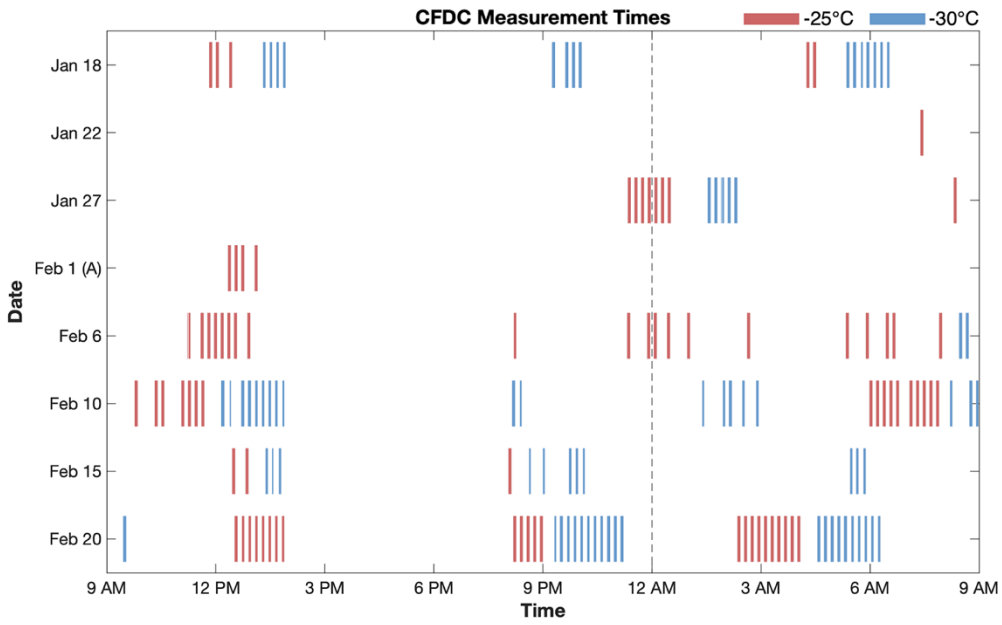

Figure 5. Times when the CFDC was collecting data at -25 °C (red bars) and -30 °C (blue bars) for the nine case dates. Each bar is roughly 5 minutes.

3.1.2 Observed vs. predicted INPs

INP concentrations predicted using the DeMott et al. (2010) parameterization were much higher than those measured by the filter and DRUM at warmer temperatures (>–20 °C; Figure 1). At colder temperatures (< –20 °C), predicted concentrations were much closer to the observed values. On some days (January 27, February 6, and February 20), predictions at –25 °C fell below the lower bound of measurement uncertainty, though still within approximately an order of magnitude. For CFDC data a -25 C and -30 C, predictions were generally within uncertainty for all sampling periods (Figure 1, 4). This parameterization was developed using CFDC measurements, which at colder temperatures (≤–20 °C) data is sparser, so the fits are less constrained. One limitation in applying this parameterization to the filter and DRUM samples is that it assumes higher particle number concentrations (>0.5 μm), as might be encountered in polluted locations relative to clean conditions, correspond to higher INP concentrations. However, previous studies in other locations have shown that INP concentrations often remain similar between clean and polluted periods (Creamean et al. 2018; McCluskey et al. 2018; Schill et al. 2016; Chen et al. 2024; Tain et al. 2022; and Cabrera-Segoviano et al., 2022). In Fairbanks, wintertime conditions are characterized by frequent pollution episodes, yet the DeMott et al. (2010) parameterization was primarily developed from CFDC measurements in more remote environments. As a result, the assumed relationship between higher particle number concentrations (>0.5 μm) and higher INP concentrations may not hold in polluted subarctic environments, particularly at warmer temperatures.

3.1.3 Focusing on INP sizes

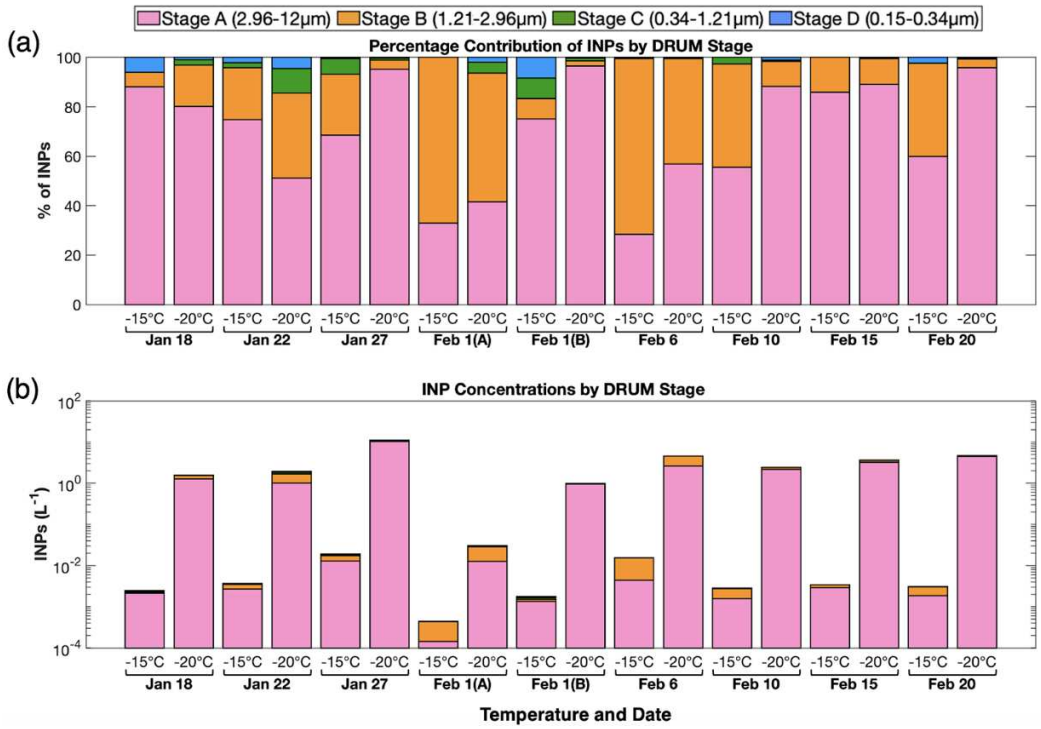

Figure 6. (a) Percentage of each DRUM stage (A-D) that contributed to the total DRUM A-D sum INPs at -15 °C and -20°C. (b) shows absolute INP concentrations for each DRUM stage (A-D) at -15 °C and -20 °C.

Figure 6 shows the size-resolved contributions to the INP population, including (a) the percentage each DRUM stage (A–D) contributed to the total DRUM A–D INPs at –15 °C and –20 °C, and (b) the corresponding absolute INP concentrations for each stage at these temperatures. As stated above, given the agreement within roughly an order of magnitude between the filter and DRUM A–D sum in Figure 1, we can assume that most INPs are represented within the DRUM A–D stages. Across all nine sampling periods, the DRUM A–D sum consistently yielded higher INP concentrations than the DRUM B–D sum, highlighting the importance of larger INPs (>1.21 μm) in Fairbanks. More specifically, greater than 80% of INPs at –15 °C and –20 °C originated from aerosols in DRUM stages A and B (1.21–12 μm), with stage A alone contributing over 50% in most cases. This finding is consistent with previous work

showing enhanced INP activity in the supermicron size range (Mason et al., 2016). Two notable exceptions to this trend occurred. During the February 1(A) ice fog period, stage A contributed only ~35% and ~40% of INPs at –15 °C and –20 °C, respectively. On February 6, stage A contributed ~30% of INPs, with the majority (>65%) found in stage B. As shown in Figure 2, this February 6 result aligns with the lowest aerosol mass concentrations among all analyzed periods and in all DRUM size ranges, and a higher mass concentration in the stage B size range (1.21–2.96 μm) compared to stage A (2.96–12 μm). Despite these exceptions, all nine sampling periods showed that ≥80% of INPs were captured in DRUM stages A and B (1.21–12 μm), even though Fairbanks' aerosol population was more heavily represented in the smaller size ranges corresponding to DRUM stages C and D (0.15–1.21 μm)

3.1.4 Ice Fog (February 1) INPs

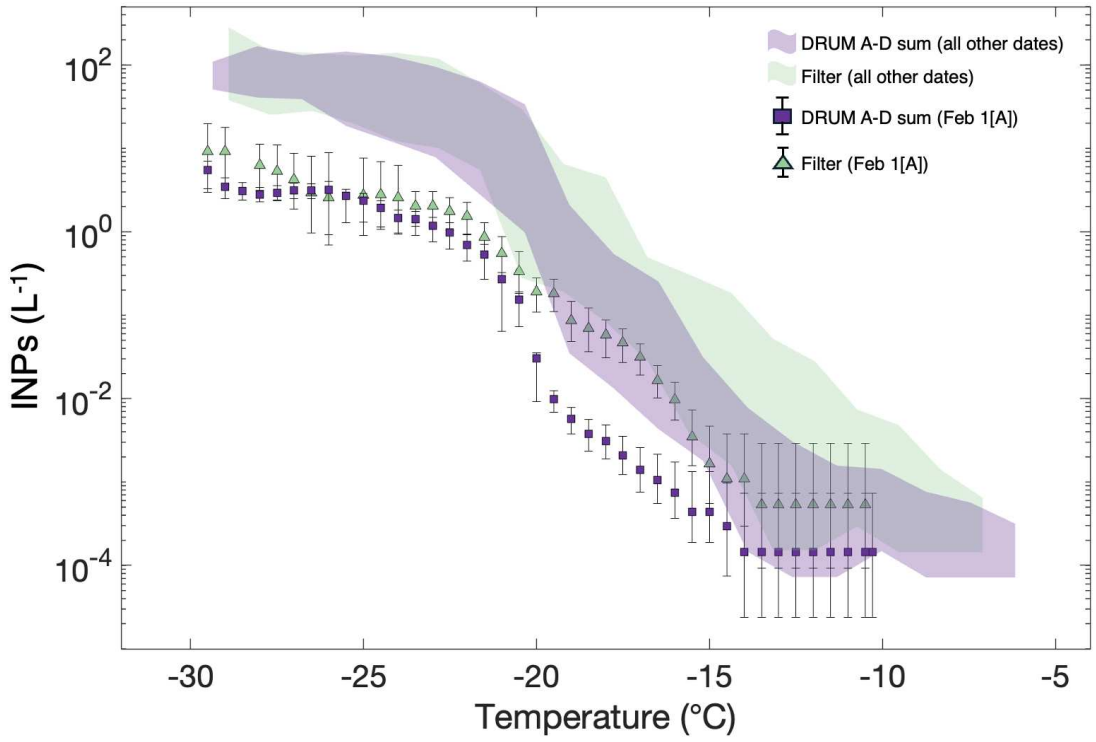

Figure 7. February 1(A) INP spectra for filter (green triangles) and DRUM A-D sum (purple squares), along with shaded INP spectra of the other eight case periods for filter (green shaded region) and DRUM A-D sum (purple shaded region).

February 1 was notable for the occurrence of an ice fog event coinciding with a high-pollution episode. During the daytime sampling period (February 1(A)), particle mass concentrations in the 0.015–12 µm range reached their highest values among all sampling periods (Figure 2). However, Figure 7 shows that INP concentrations for both the filter and DRUM A–D were the lowest across all temperatures colder than –15 °C compared to the other eight periods.

At –25 °C, agreement among all three instruments was close within uncertainty bounds (95% CI): the CFDC measured 2–9 INPs L^{-1} during its sampling times, the filter recorded an

average of 3 INPs L^{-1}, and the DRUM A–D and B–D sums both measured around 2 INPs L^{-1} (Figure 4). Given the presence of ice fog, actual INP concentrations were likely higher near the onset of the event. With ambient temperatures near or below −30 °C, many INPs, particularly those active at warmer temperatures, may have already nucleated ice by the time sampling occurred and therefore were not detected by the instruments (Lill et al., 2024). From Figure 6, DRUM A–D had its lowest INP concentrations during this event at –15 °C and –20 °C, with the majority of INPs originating from stage B. Given that the CFDC and DRUM stage B have similar upper size cut-offs, it is reasonable to assume that most INPs captured by the filter during this period were also within this size range. These INPs likely remained interstitial during sampling within the ice fog.

3.2 Aerosol Composition

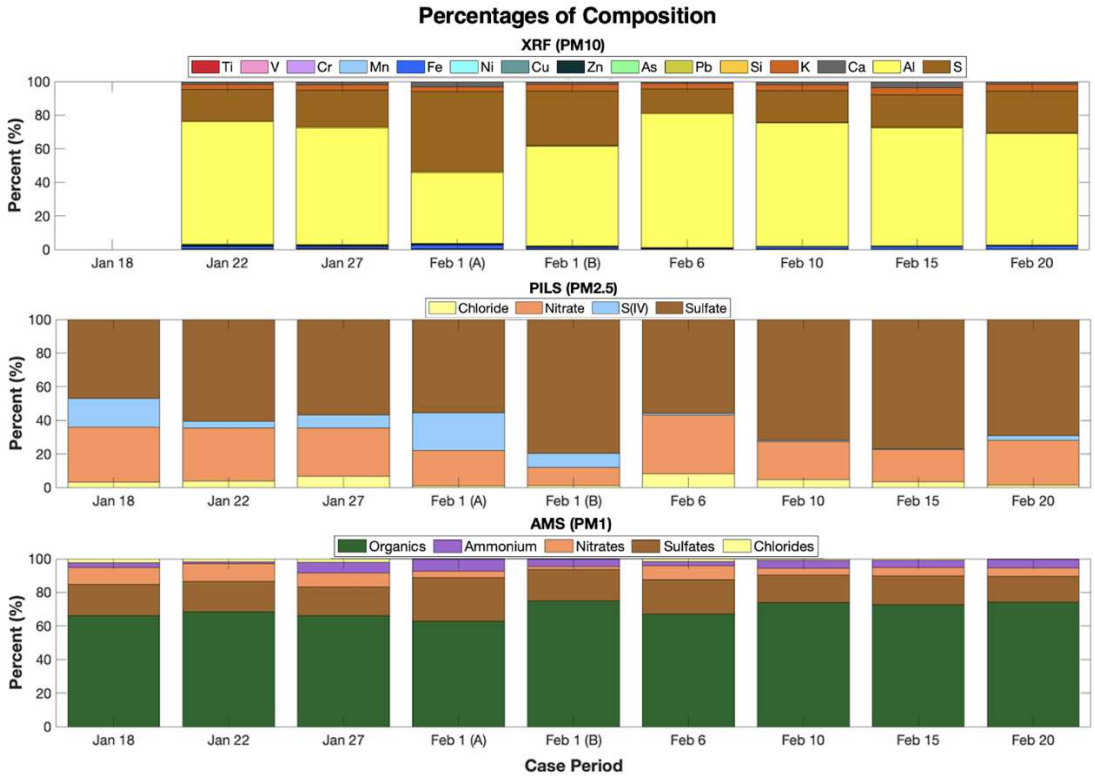

Figure 8. The percent aerosol composition from three different instruments that each have three different size cuts. (top panel) XRF: PM10; (middle panel) PILS: PM2.5; and (bottom panel) AMS: PM1

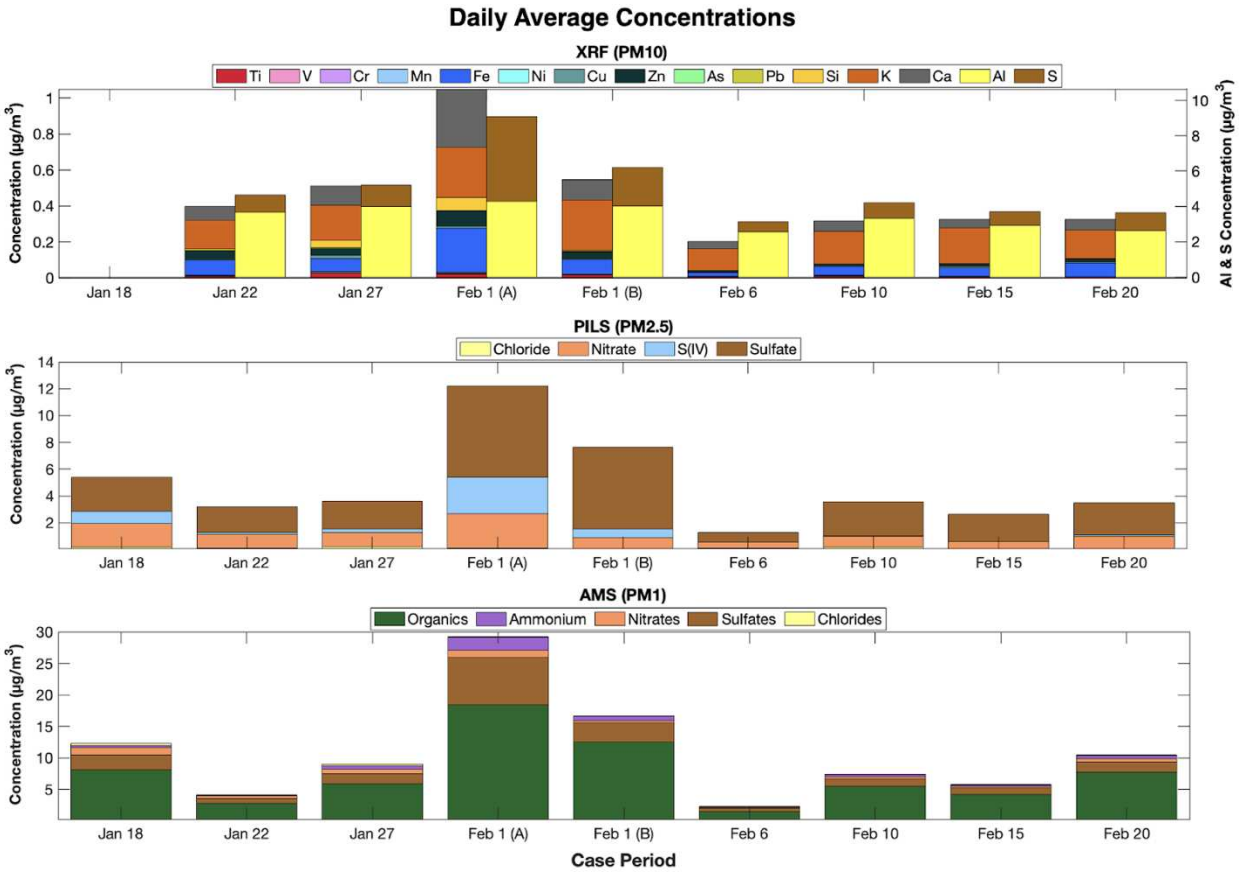

Figure 9. As in Figure 7 but for the daily average concentrations in µg m^{-3}.

Figures 8 and 9 show the aerosol composition for the nine case dates. The PM_1 fraction, as measured by the AMS, was dominated by organics and sulfate. The AMS organics reflect a combination of primary emissions from residential wood burning and oxygenated organic aerosol associated with the atmospheric processing of these emissions, as observed during the ALPACA campaign in Fairbanks (Ijaz et al., 2024). In the $PM_{2.5}$ fraction, measured by PILS-IC, sulfate contributions were larger relative to PM_1, with most of this sulfate attributed to residential fuel oil combustion during the campaign (Moon et al., 2023). PILS-IC measures soluble ions, so these values represent only the water-soluble fraction of $PM_{2.5}$. In contrast, the PM_{10} fraction, measured by XRF, was dominated by aluminum and sulfur. The aluminum signal has been identified as a dust signature (Lill et al., 2024; Costa et al., 2025). XRF measures elemental

concentrations, which include both soluble and insoluble components, and the PM_{10} size cut captures a broader particle population than $PM_{2.5}$. As a result, differences between the $PM_{2.5}$ and PM_{10} composition reflect both chemical speciation and size-dependent source contributions.

While absolute aerosol mass concentrations varied between case periods (Figure 9), the percent composition remained broadly similar across dates (Figure 8). Feb 1(A) is not anomalous in its fractional makeup, but it stands out because absolute concentrations in all three size fractions are the highest of the campaign (Figure 9). The increase was driven mainly by organics in PM_1 and sulfate in $PM_{2.5}$. This period coincided with the high-pollution ice fog event described in Section 3.1.4, during which the extremely cold temperatures led to increased residential wood burning and higher emissions from coal-fired power plants to meet energy demands.

3.3 Assessing INP composition and potential local sources

To investigate the composition of size-resolved INPs, we analyzed a subset of DRUM samples from January 22, February 1, and February 6, 2022. These dates were selected to represent near-average, high, and low pollution conditions, respectively, based on ambient aerosol number and mass concentrations. Corresponding filter samples were also analyzed for comparison. Heat and peroxide treatments were applied to distinguish between heat-labile organics, heat-stable organics, and inorganics, allowing for an assessment of the dominant INP types and their potential sources (Hill et al. 2016). Figures 10 and 11 show the fractional contributions of each INP type at three freezing temperatures for the filter and DRUM samples, respectively. This is the first time INP treatments have been conducted on size-resolved samples.

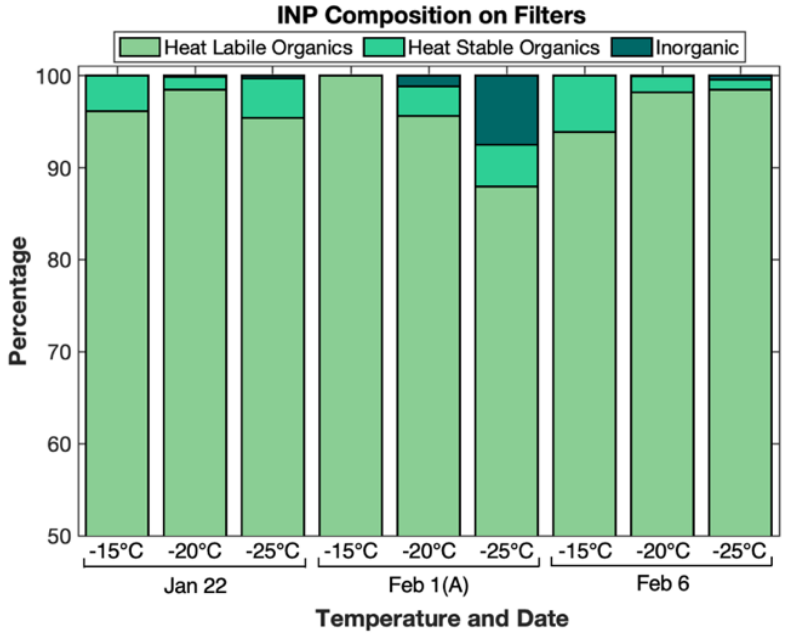

Figure 10. Percent of INPs that are heat-labile organic, heat-stable organic, and inorganic for INPs active at three freezing temperatures in the filter samples from three case periods.

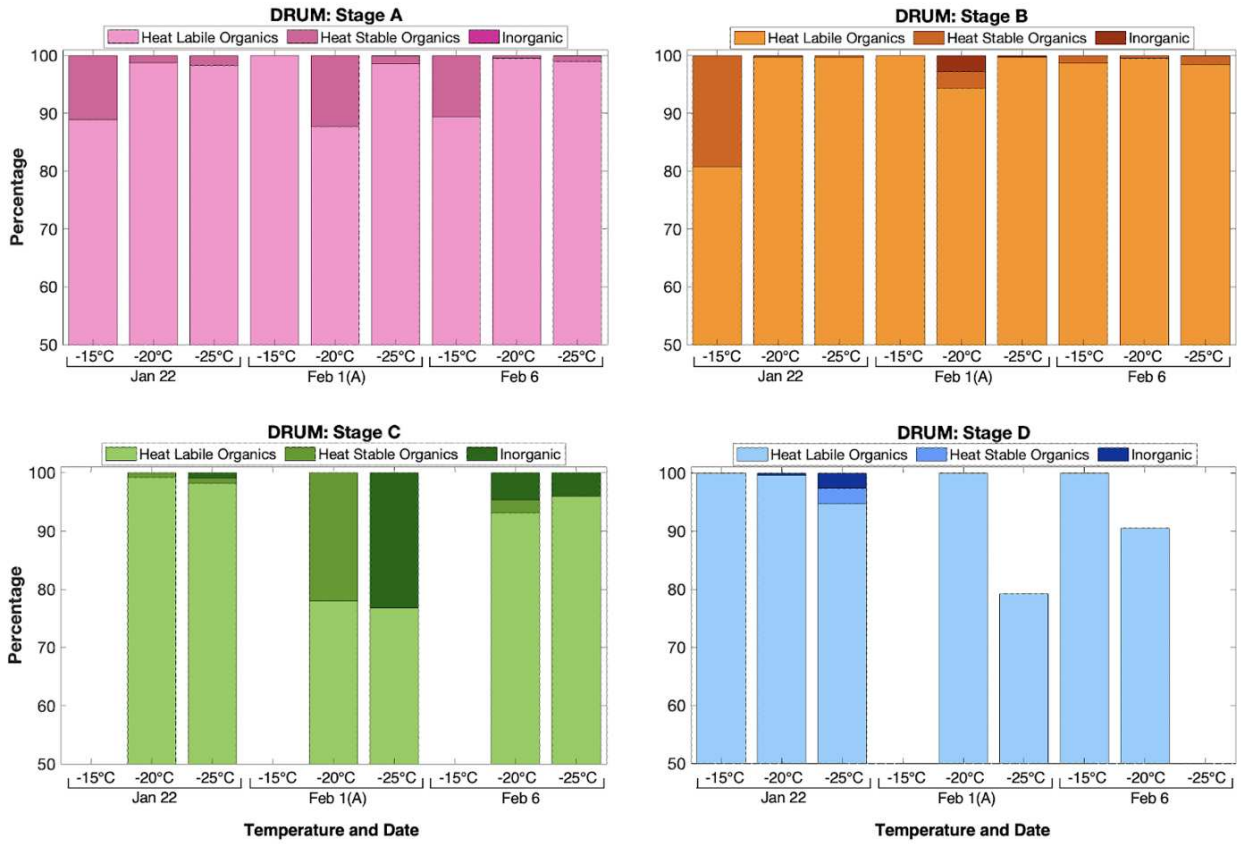

Figure 11. Percent of INPs that are heat-labile organic, heat-stable organic, and inorganic for INPs active at three freezing temperatures in the DRUM (A-D) samples from three case periods.

3.3.1 Heat-Labile Organic INPs

Heat-labile organic INPs were the dominant contributor at all three freezing temperatures for the three case dates examined (Figures 10 and 11). On the filters, they accounted for over 90% of INPs at –15 °C and –20 °C, and they comprised the majority across all DRUM stages. These INPs are commonly linked to proteinaceous or other biological materials (Hill et al., 2016; O'Sullivan et al., 2018; Suski et al., 2018). While primary biological INPs may seem unlikely during Fairbanks' mid-winter conditions given the frozen, snow-covered landscape, similar results were reported by Lill et al. (2024), who conducted heat treatments on filters across eight different 24-hr sampling periods during ALPACA. Their results showed heat labile organic INPs were a dominant contributor to the INP population on all days studied and they also observed a reduction in these INPs on January 31 at -20 °C and -25 °C during the same ice fog. Despite the freezing temperatures and snow/ice covered surfaces, a previous study that took place in spring near Oliktok Point, located on the northern Alaskan coast, showed that local and regional transport from marine and terrestrial sources can contribute coarse-mode, warm-temperature INPs, potentially of biological origin (Creamean et al. 2018). However, Fairbanks lacks direct marine influence, and with frequent wintertime inversions, local sources are expected to strongly dominate as capping inversions are strong and frequent (Cesler-Maloney et al., 2022).

A plausible local source of heat-labile INPs in Fairbanks could be lichens (Eufemio et al. 2024; Macander et al. 2020), which commonly grow on trees in the area and would remain exposed during winter. Lichens are symbiotic organisms composed of fungi and photosynthetic partners (algae and/or cyanobacteria), capable of surviving extreme environmental conditions, including freezing, and are known to act as efficient INPs at relatively warm temperatures (≥ -5 °C) (Kieft, 1988). In a recent study, Eufemio et al. (2023) collected lichen samples from various

Alaskan regions in September 2021 and February 2022, including two species from Fairbanks. They found that 50% of droplets in their assay that contained the lichen species *Usnea wirthii* froze by -8.2 °C, while the *Bryoria* species reached 50% freezing at -14.5 °C. The study also demonstrated the persistence of INP activity in lichens, with multiple freeze-thaw cycles having minimal effect on their ice-nucleating efficiency.

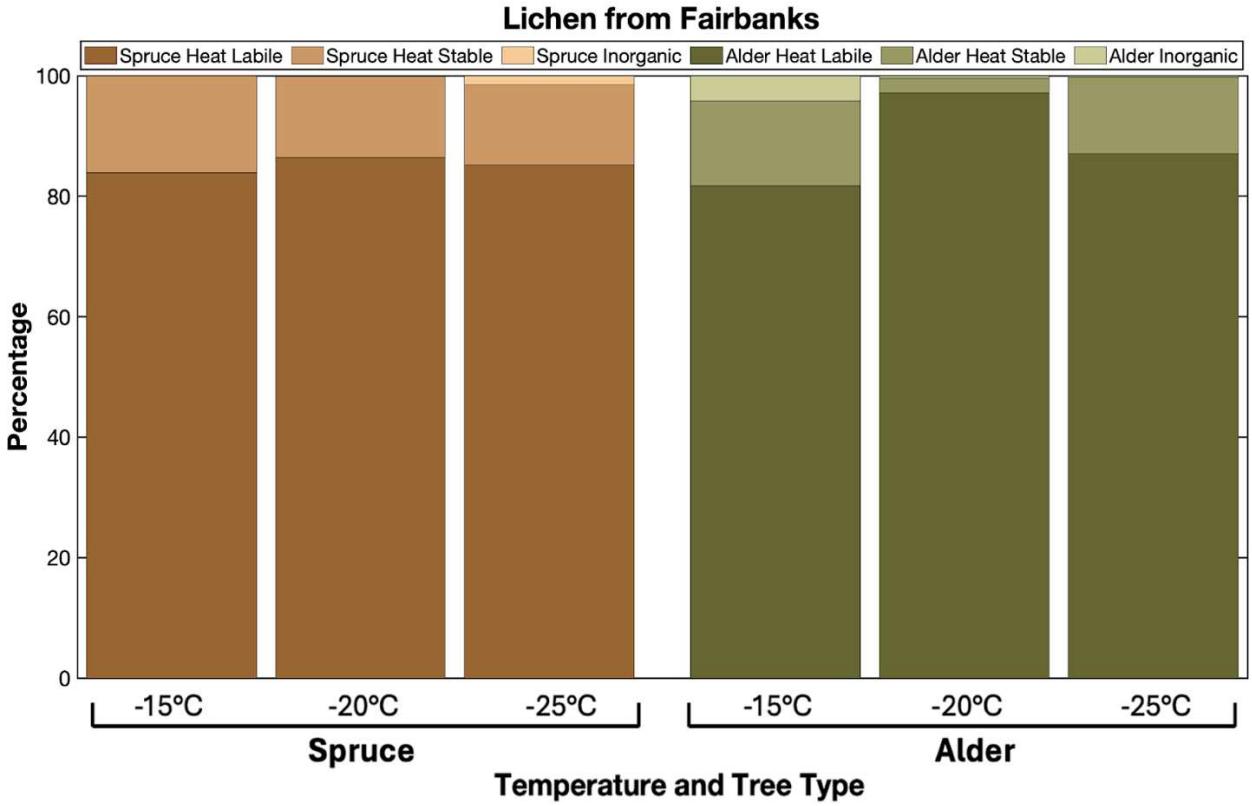

Figure 12. Percent of INPs that are heat labile organic, heat stable organic, and inorganic across three freezing temperatures for lichen samples collected from spruce (brown, left panels) and alder (green, right panels) trees.

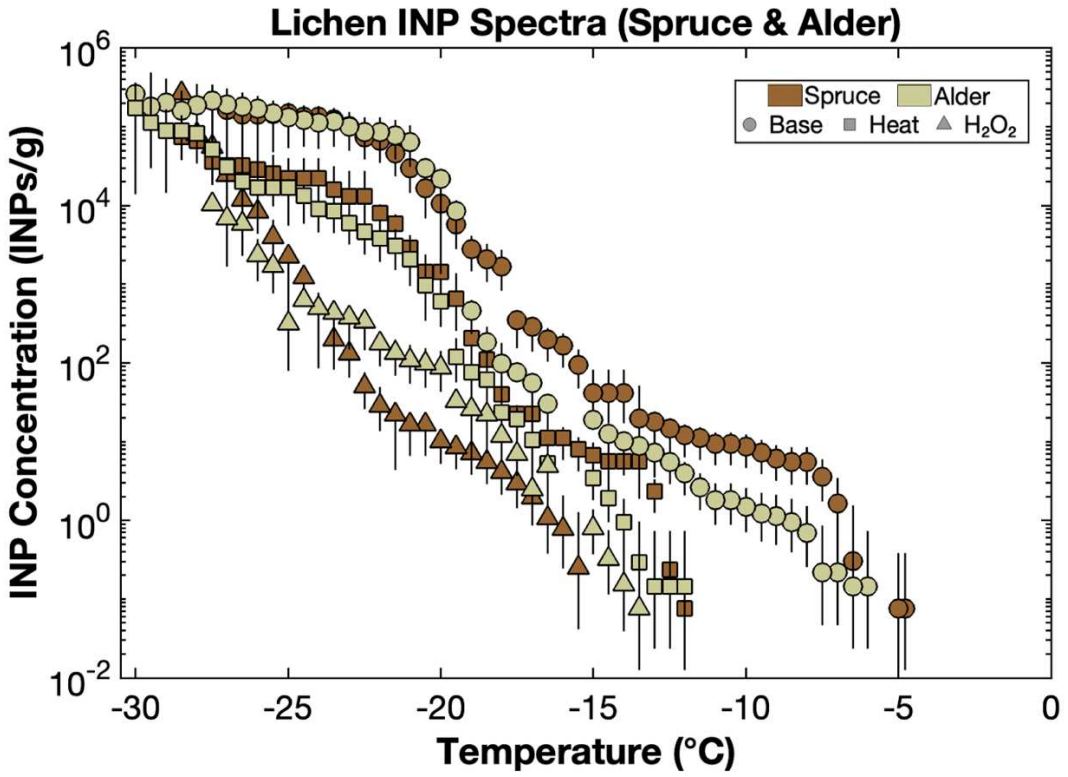

Figure 13. INP spectra of lichen samples collected from spruce (brown) and alder (green) trees. The circles represent the base spectra, the squares represent the heat treatments, and the triangles are the peroxide treatment.

To further investigate this potential source of heat-labile INPs, lichen samples were collected from both spruce and alder trees in Fairbanks and INP spectra measured as discussed above. As shown in Figure 12, more than 80% of INPs from both spruce- and alder-associated lichen washings were heat-labile at -15 °C, -20 °C, and -25 °C. Notably, Figure 13 reveals an onset freezing temperature between approximately -7 °C and -5 °C for the untreated (base) lichen samples. Following heat treatment, the majority of INPs active between -5 °C and -12 °C were eliminated, indicating their sensitivity to heating and confirming they are likely of biological nature. Given that lichen are abundant in Fairbanks and resilient to cold temperatures, lichen could be a potential source of the airborne heat-labile organic INPs found on the filter and DRUM samples.

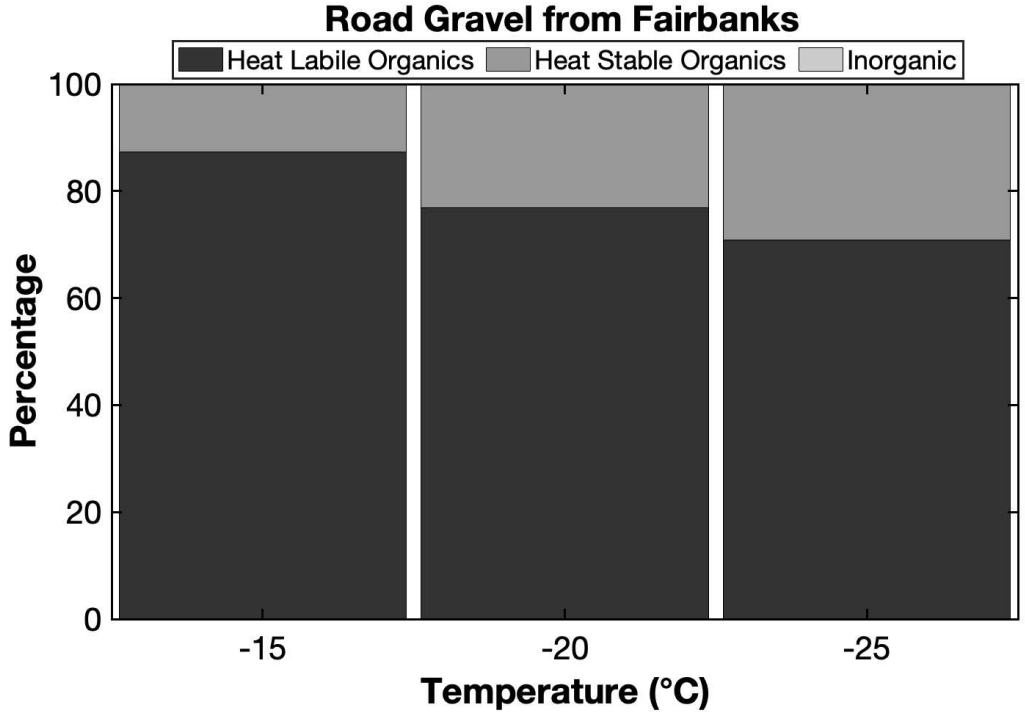

Figure 14. Percent of INPs that are heat labile organic, heat stable organic, and inorganic across three freezing temperatures for the road gravel sample.

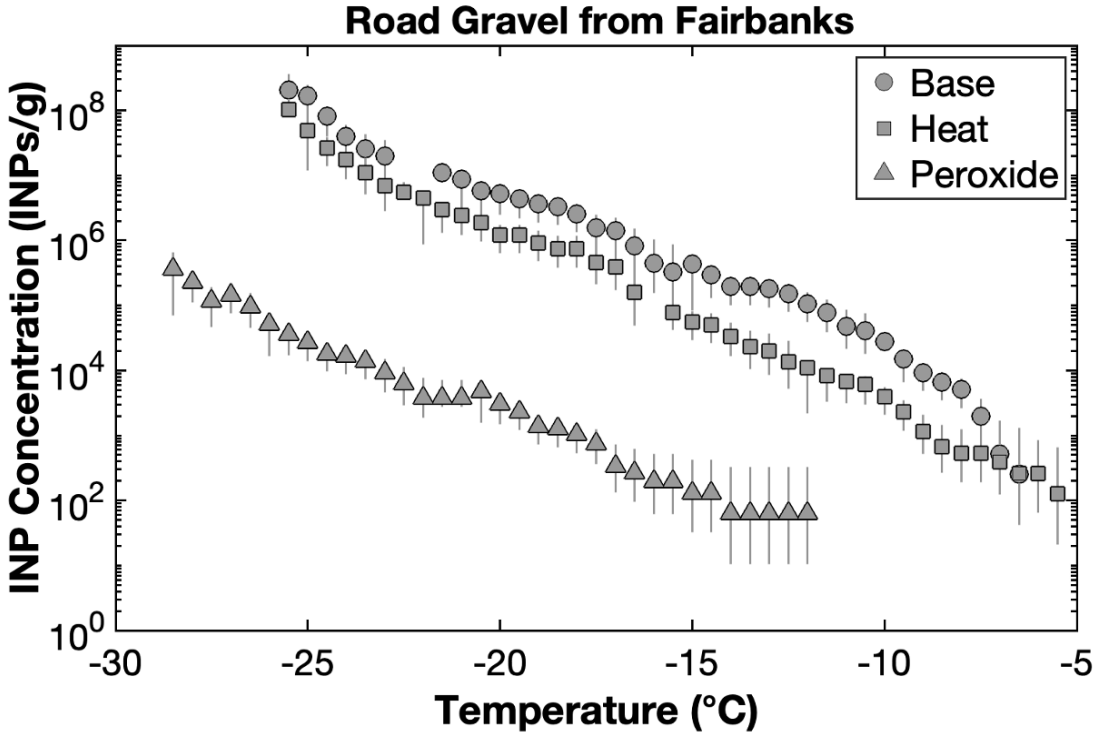

Figure 15. INP spectra of road gravel for the base/untreated (circle), heat treated (square) and peroxide treated (triangle) samples.

A fraction of the heat-labile organic INPs, particularly in the larger particle size ranges collected on the filter and DRUM stages A and B, may originate from dust, as also hypothesized by Lill et al. (2024). Interestingly, a recent study from Costa et al. (2025) found that dust was the most abundant particle type found in ice crystal residual samples collected during the same ice fog event during ALPACA (61-63%). One plausible source of dust in Fairbanks is road gravel. Due to extremely cold conditions in Fairbanks winter, road salt becomes ineffective as a de-icer, leading to the increased use of road gravel. This gravel can acquire organic and/or biological material through environmental exposure, such as airborne deposition onto gravel stockpiles or through direct human handling. As shown in Figure 14, a significant fraction (>60% and >80%) of INPs from road gravel washings were heat-labile at -15 °C and -25 °C respectively.

Costa et al. (2025) showed that following the large percentage of dust in ice fog residuals were organic particles (23-27%), and the least represented was biological (5-9%) across four size bins ranging from 1.8-18 μm, which seemingly disagrees with our treatment results. The difference in the estimated contributions from heat-labile /heat-stable organic INPs during the ice fog event (February 1(A)) between this study and Costa et al. (2025) can be attributed to the different sampling types. Costa et al. (2025) sampled ice crystals within the ice fog itself, when temperatures were near or below -30 °C, colder than the CSU IS could reach in this study, and identified particle types from the residuals after water was evaporated. In addition, our INP identification technique isolated INPs active in the immersion freezing mode, whereas another freezing mode could be at play at temperature below -30°C. Lastly, the high abundance of dust and organic particles reported by Costa et al. (2025) may still include heat-labile components. Their classification of “biological” INPs required the identification of whole biological particles, whereas biological INP activity can also originate from cell-free fragments, proteins, or

biological material attached to dust. These sources would likely have been grouped into the "dust" or "organic" categories in their analysis, providing another explanation for the apparent disagreement with our heat-treatment results.

3.3.2 Heat-Stable Organic INPs

Heat-stable organics, representing non-proteinaceous organic material, comprised a relatively small fraction of the total INP population. In DRUM stage A, organics contributed 0-12% across all temperatures and sampling dates shown in Figure 11, with slightly higher contributions observed in stage B (0-20%) and stage C (0-22%), and the lowest contributions in stage D (0-3%). The filters in this study also showed approximately 5% of INPs as heat-stable organics during the ice fog event (February 1(A)) at -25 °C (Figure 10). Costa et al. (2025) reported that 23-27% of ice fog residuals were organic particles, though their analysis focused on particles between 1.8-18 μm. This size range is most representative of DRUM stage A, partially representative of stage B, and does not capture the smaller sizes associated with stages C and D, or the full range collected on the filters. Additionally, the temperatures during ice fog residual sampling were substantially colder (≤ –30°C), which as discussed in Section 3.3.1, may influence the freezing mode compared to conditions applied in our measurements and analyses. Overall, the compositional analysis, particularly heat and peroxide treatments, suggest that much of the INP activity in the immersion freezing mode, can be attributed to local organic sources, including biological material such as lichen and/or local dust-related mineral INPs from sources that include road gravel with associated organic content.

3.3.3 Inorganic INPs

A small contribution to INPs from inorganic particles was observed in both the filter samples and DRUM stages (Figures 10 and 11). While DRUM stage A showed no detectable inorganic INPs, stages B, C, and D exhibited small percentages (0-3%, 0-24%, and 0-3% respectively). The highest inorganic fractions were observed on February 1(A), during the ice fog event, at –25°C, with ~7.5% in the filters and ~24% in DRUM stage C. Although this appears as an increase in the inorganic fraction, it most likely reflects a relative decrease in other INP types, since many particles were already nucleated within the ice fog and removed from the interstitial phase. This elevated inorganic presence, compared to the other two case periods analyzed for composition, is consistent with the findings of Lill et al. (2024), who reported a ~30% inorganic fraction at –25°C from filter samples collected the previous day (January 31). They suggested that this increase in inorganics during the ice fog, compared to pre/post-ice fog, could be due to an enhanced source of inorganic aerosols during the coldest period of the campaign and/or a lower activation efficiency. To support the presence of a heightened source of inorganics, elevated sulfur and sulfate concentrations measured by both XRF and PILS on this day (Figures 8 and 9) suggested increased emissions, and/or increased trapping of emissions during the event. These elevated levels may have resulted from both increased residential wood burning and emissions from coal-fired power plants in Fairbanks (Moon et al. 2023). Chen et al. (2025), showed that inorganic ash and mineral phases from biomass burning, rather than the carbonaceous fraction, are the likely contributors to biomass burning INPs.

3.4 Comparing INPs from ALPACA with other Urban and/or Arctic Locations

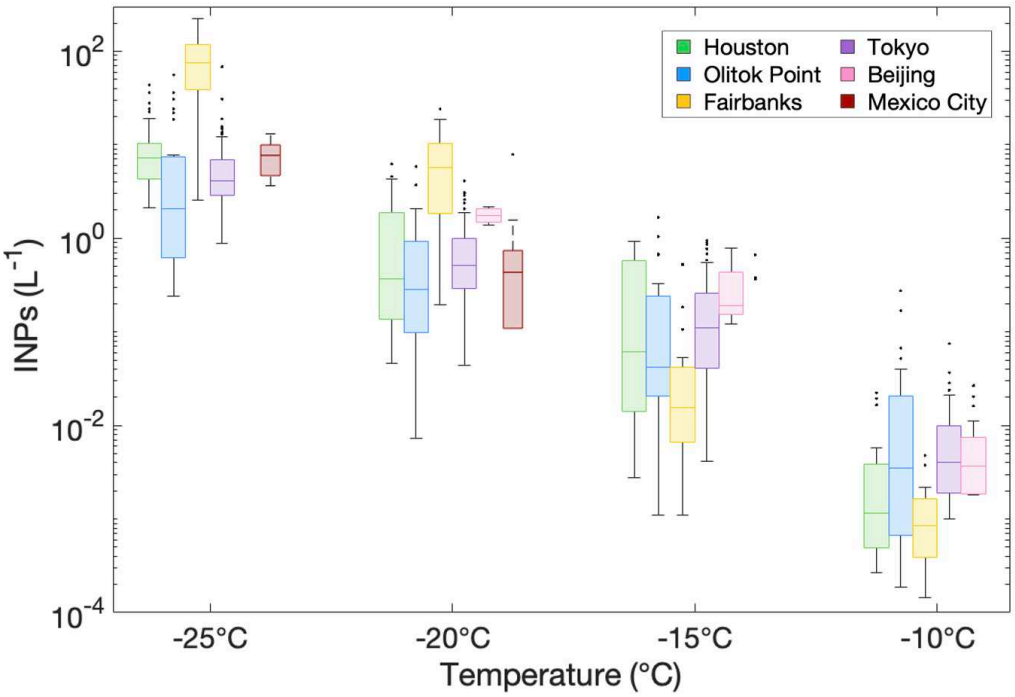

Figure 16. Reported INPs during summer months: Houston (Shi et al. 2022), Beijing (Chen et al. 2024), and Mexico City (Cabrera-Segoviano et al. 2022); winter months: Fairbanks (this study) and year-round: Olitok Point (Creamean et al. 2018), and Tokyo (Tobo et al. 2020).

To compare how Fairbanks relates to other polluted and/or Arctic locations, we compiled data from five other studies (Figure 16). In winter, during the ALPACA campaign, Fairbanks INP concentrations tended to be higher at colder temperatures but lower at warmer temperatures compared to the other locations. At Oliktok Point, where data were collected year-round, INP concentrations peaked during the summer months, which is typical for an Arctic coastal location (Creamean et al., 2019; Wex et al., 2019). In Tokyo, which was also sampled year-round, INP concentrations showed little seasonal variation. In Mexico City, Beijing, and Houston, where sampling occurred during summer months, INP concentrations at −20 °C and −25 °C were comparable to one another, despite differences in potential emission sources. In Tokyo, INPs were largely influenced by Asian dust plumes, whereas Beijing's INPs originated primarily from

anthropogenic dust (Tobo et al., 2020; Chen et al., 2024). In Houston, sources were likely a combination of marine aerosols and anthropogenic emissions (Shi et al., 2022).

As mentioned in Section 1, some of these previous studies showed anthropogenic pollution alone often resulted in little to no change in INP concentrations between clean and polluted periods. Our results from Fairbanks in winter, based on the size and composition analyses discussed in Sections 3.1 and 3.3, provide further insight by showing that INPs were influenced primarily by surrounding natural sources, including dust and biological materials such as lichens. These regional differences highlight the importance of understanding how particle size, composition, and source origin, whether local or transported, influence INP concentrations and freezing mechanisms.

4. Conclusions

In this study we report on the concentrations, size and composition of INPs observed in a wintertime study in Fairbanks, Alaska. Despite the overall aerosol population being dominated by smaller particles ($\leq 1.21\mu m$) for both number and mass concentrations, the aerosols in the 1.21-12 μm range were consistently the dominant contributors to INP populations, confirming our first hypothesis. Analysis of three case periods with INP compositional treatments (heat and peroxide) indicated that much of the INP activity was linked to local organic sources. This finding confirms our second hypothesis and suggests that local aerosols, including biological and organic material such as lichens and dust-related mineral INPs from road gravel, were likely contributors to the observed INP activity.

These results challenge the assumption that polluted environments dominated by combustion-derived aerosols lack efficient INPs. Instead, our findings indicate that even under conditions of poor air quality, local sources such as biological material or mineral-organic

mixtures can play a substantial role in ice nucleation. This finding has important implications for understanding aerosol–cloud interactions in high-latitude urban settings and in other regions with frequent poor air quality. It also supports improvements to INP parameterizations that predict concentrations from aerosol number, especially at warmer temperatures. By characterizing both the size and composition of INPs in Fairbanks during winter, this study fills a gap in current knowledge and highlights the importance of local and seasonal variability in assessing INP sources and their climate relevance. Comparisons with other locations further demonstrate that urban and/or Arctic environments, despite their unique aerosol profiles, can harbor diverse and efficient INP populations. A clearer understanding of these factors is essential for improving predictions of INP variability across diurnal and seasonal timescales and will aid in improving our ability to predict aerosol–cloud interactions, including effects on cloud lifetime, precipitation, and radiative forcing.

5. Future Work

This study highlights the limited availability of size- and composition-resolved INP measurements, not only in cold, polluted urban environments like Fairbanks but also in rural and remote locations with cleaner air. A key limitation was the challenge of comparing filter INPs to the DRUM A–D sum due to their different size-capturing abilities (filter: total aerosol; DRUM A–D: 0.15 to 12 μm) and the difficulty of detecting large particles (12 to 34 μm) with the OPC because of inlet losses and their naturally low abundance in Fairbanks. A potential improvement would be to include a third offline impactor, such as a MOUDI, which can capture a broader particle size range for INP analysis, including beyond the DRUM upper limit (>12 μm). This would allow for more complete instrument intercomparisons and, if the MOUDI offers finer size resolution, could better pinpoint INP size distributions in other locations.

Performing heat and peroxide treatments, as in this study, on both DRUM and MOUDI samples would further resolve INP composition by size. Past work, such as Maki et al. (1974), demonstrated that additional treatments such as dyes, antibiotics, and chemical agents can diminish INP activity in certain biological species like Pseudomonas syringae, which is active at very warm temperatures (−1.8 to −3.8 °C). While some dyes, including crystal violet and safranin, lowered freezing temperatures to around −17 °C, treatment effectiveness varies between species because of differences in cell wall structure. Developing a method that can further divide heat-labile, heat-stable, and inorganic INPs into smaller subcategories would provide valuable insight for future size-resolved studies. Given the prevalence of wood burning in Fairbanks during winter, if wood combustion samples from common fuels such as birch were analyzed with heat and peroxide treatments described in this paper, we would expect the majority of the INP activity to remain in the inorganic/heat-stable fraction. It is possible wood burning could contribute to the small fractions of inorganic INPs observed during ALPACA.

Future research should also aim for higher temporal resolution to capture diurnal and short-term variations in INP concentrations and compositions. For example, dividing 24-hour samples into 8am–8pm versus 8pm–8am would allow comparisons between periods of active emissions and those with reduced activity. Achieving this resolution would require pulling larger volumes of air in shorter collection windows, which in turn would require a high-flow pump to ensure sufficient air mass is collected for filter analysis. This approach would better isolate the influence of human activity and boundary layer dynamics on INP variability, helping to distinguish between peak emission periods and more stable nighttime conditions. Coupling these observations with meteorological analyses such as inversion height would help in locations that experience frequent inversions like Fairbanks and see if that places a role in the abundance of

INPs. Together, these approaches would extend the findings of this thesis and improve predictions of how INP populations respond to varying atmospheric conditions, which is essential for better representation in weather and climate models.

References

Agresti, A, and BA Coull. 1998. “Approximate Is Better than ‘Exact’ for Interval Estimation of Binomial Proportions.” The American Statistician 52(2): 119–126, https://doi.org/10.2307/2685469

Air Pollution. World Health Organization. (n.d.). https://www.who.int/health-topics/air-pollution#tab=tab_1

Barry, K. R., Hill, T. C. J., Jentzsch, C., Moffett, B. F., Stratmann, F., & DeMott, P. J. (2021a). Pragmatic protocols for working cleanly when measuring ice nucleating particles. *Atmospheric Research*, **250**, 105419. https://doi.org/10.1016/j.atmosres.2020.105419

Berezinski, N. A., Stepanov, G. V., and Khorguani, V. G.: Ice- forming activity of atmospheric aerosol particles of different sizes, Lecture Notes in Physics, edited by: Wagner , P. E. and- Vali, G., 309, 709–712, Springer, Heidelberg and Berlin, Ger- many, 1988.

Bi, K., et al., Continuous measurements of ice nucleating particles in Beijing, China, submitted to Geophysical Research Letters, 2018.

Brett, N., Arnold, S. R., Law, K. S., Raut, J.-C., Onishi, T., Barret, B., Dieudonné, E., Cesler-Maloney, M., Simpson, W., Bekki, S., Savarino, J., Albertin, S., Gilliam, R., Fahey, K., Pouliot, G., Huff, D., & D’Anna, B. (2025). Estimating power plant contributions to surface pollution in a wintertime Arctic environment. ACS ES&T Air, 2(5), 943–956. https://doi.org/10.1021/acsestair.5c00030

Cabrera-Segoviano, D., Pereira, D. L., Rodriguez, C., Raga, G. B., Miranda, J., Alvarez-Ospina, H., & Ladino, L. A. (2022). Inter-annual variability of ice nucleating particles in Mexico City. Atmospheric Environment, 281, 118964. https://doi.org/10.1016/j.atmosenv.2022.118964

Campbell, J. R.; Battaglia, M.; Dingilian, K.; Cesler-Maloney, M.; St Clair, J. M.; Hanisco, T. F.; Robinson, E.; DeCarlo, P.; Simpson, W.; Nenes, A.; Weber, R. J.; Mao, J. Source and Chemistry of Hydroxymethanesulfonate (HMS) in Fairbanks, Alaska. *Environ. Sci. Technol.* **2022**, *56* (12), 7657– 7667, DOI: 10.1021/acs.est.2c00410

Cesler-Maloney, M., Simpson, W. R., Miles, T., Mao, J., Law, K. S., & Roberts, T. J. (2022). Differences in ozone and particulate matter between ground level and 20 m aloft are frequent during wintertime surface-based temperature inversions in Fairbanks, Alaska. *Journal of Geophysical Research: Atmospheres*, **127**(10), e2021JD036215. https://doi.org/10.1029/2021JD036215

Chen, J., Wu, Z., Gong, X., Qiu, Y., Chen, S., Zeng, L., & Hu, M. (2024). Anthropogenic dust as a significant source of ice-nucleating particles in the urban environment. *Earth's Future*, **12**(1), e2023EF003738. https://doi.org/10.1029/2023EF003738

Chen, J., Martin Othmar Jakob, F., Voliotis, A., Wu, H., Aisyah Syafira, S., Oghama, O., Shardt, N., Fauré, N., Kong, X., Mcfiggans, G., & A. Kanji, Z. (2025). Ice Nucleation Abilities and Chemical Characteristics of Laboratory-Generated and Aged Biomass Burning Aerosol. https://doi.org/10.5194/egusphere-egu25-6935

Clarke, A. D., Shinozuka, Y., Kapustin, V. N., Howell, S., Hue- bert, B., Doherty, S., Anderson, T., Covert, D., Anderson, J., Hua, X., Moore II, K. G., McNaughton, C., Carmichael, G., and We- ber, R.: Size distributions and mixtures of dust and black carbon aerosol in Asian outflow: Physiochemistry and optical properties, J. Geophys. Res., 109, D15S09, doi:10.1029/2003JD004378, 2004.

Conen, F., Morris, C. E., Leifeld, J., Yakutin, M. V., & Alewell, C. (2011). Biological residues define the ice nucleation properties of soil dust. *Atmospheric Chemistry and Physics*, 11, 9643–9648. https://doi.org/10.5194/acp-11-9643-2011

Creamean, J. M., Kirpes, R. M., Pratt, K. A., Spada, N. J., Maahn, M., de Boer, G., Schnell, R. C., & China, S. (2018). Marine and terrestrial influences on ice nucleating particles during continuous springtime measurements in an Arctic oilfield location. *Atmospheric Chemistry and Physics*, 18, 18023–18042. https://doi.org/10.5194/acp-18-18023-2018

Creamean, J. M., Mignani, C., Bukowiecki, N., & Conen, F. (2019). Using freezing spectra characteristics to identify ice-nucleating particle populations during the winter in the Alps. Atmospheric Chemistry and Physics, 19(12), 8123–8140. https://doi.org/10.5194/acp-19-8123-2019

Creamean, J. M., Hill, T. C. J., & Hume, C.(2022b). Ice Nucleation Spectrometer (INS) instrument handbook. https://doi.org/10.2172/1846263

Daily, M. I., Tarn, M. D., Whale, T. F., & Murray, B. J. (2022). An evaluation of the heat test for the ice-nucleating ability of minerals and biological material. Atmospheric Measurement Techniques, 15(8), 2635–2665. https://doi.org/10.5194/amt-15-2635-2022

DeMott, P. J., Prenni, A. J., Liu, X., Kreidenweis, S. M., Petters, M. D., Twohy, C. H., ... & Rogers, D. C. (2010). Predicting global atmospheric ice nuclei distributions and their impacts on climate. Proceedings of the National Academy of Sciences, 107(25), 11217–11222. https://doi.org/10.1073/pnas.0910818107

DeMott, P. J., Mason, R. H., McCluskey, C. S., Hill, T. C. J., Perkins, R. J., Desyaterik, Y., et al. (2018). Ice nucleation by particles containing long-chain fatty acids of relevance to freezing by sea spray aerosols. *Environmental Science: Processes and Impacts*, **20**(11), 1559–1569. https://doi.org/10.1039/C8EM00386F

Després, V. R., Huffman, J. A., Burrows, S. M., Hoose, C., Safa- tov, A. S., Buryak, G., Fröhlich-Nowoisky, J., Elbert, W., An- dreae, M. O., Pöschl, U., and Jaenicke, R.: Primary biological aerosol particles in the atmosphere: a review, Tellus B, 64, 15598, doi:10.3402/tellusb.v64i0.15598, 2012.

Eufemio, R. J., de Almeida Ribeiro, I., Sformo, T. L., Laursen, G. A., Molinero, V., Fröhlich-Nowoisky, J., Bonn, M., & Meister, K. (2023). Lichen species across Alaska produce highly active and stable ice nucleators. *Biogeosciences*, *20*(13), 2805–2812. https://doi.org/10.5194/bg-20-2805-2023

Elbert, W., Taylor, P. E., Andreae, M. O., and Pöschl, U.: Contribu- tion of fungi to primary biogenic aerosols in the atmosphere: wet and dry discharged spores, carbohydrates, and inorganic ions, At- mos. Chem. Phys., 7, 4569–4588, doi:10.5194/acp-7-4569-2007, 2007.

Graham, B., Guyon, P., Maenhaut, W., Taylor, P. E., Ebert, M., Matthias-Maser, S., Mayol-Bracero, O. L., Godoi, R. H. M., Artaxo, P., Meixner, F. X., Moura, M. A. L., Rocha, C. H. E. D., Van Grieken, R., Glovsky, M. M., Flagan, R. C., and Andreae, M. O.: Composition and diurnal variability of the natural Amazonian aerosol, J. Geophys. Res., 108, 4765, doi:10.1029/2003JD004049, 2003.

Hill, T. C. J., DeMott, P. J., Tobo, Y., Fröhlich-Nowoisky, J., Moffett, B. F., Franc, G. D., & Kreidenweis, S. M. (2016). Sources of organic ice nucleating particles in soils. *Atmospheric Chemistry and Physics*, **16**(11), 7195–7211. https://doi.org/10.5194/acp-16-7195-2016

Hoose, C., & Möhler, O. (2012). Heterogeneous ice nucleation on atmospheric aerosols: A review of results from laboratory experiments. *Atmospheric Chemistry and Physics*, **12**(20), 9817–9854. https://doi.org/10.5194/acp-12-9817-2012

Huffman, J. A., Sinha, B., Garland, R. M., Snee-Pollmann, A., Gunthe, S. S., Artaxo, P., Martin, S. T., Andreae, M. O., and Pöschl, U.: Size distributions and temporal variations of bio- logical aerosol particles in the Amazon rainforest characterized by microscopy and real-time UV-APS fluorescence techniques during AMAZE-08, Atmos. Chem. Phys., 12, 11997–12019, doi:10.5194/acp-12-11997-2012, 2012.

Huffman, J. A., Prenni, A. J., DeMott, P. J., Pöhlker, C., Mason, R. H., Robinson, N. H., Fröhlich-Nowoisky, J., Tobo, Y., Després, V. R., Garcia, E., Gochis, D. J., Harris, E., Müller-Germann, I., Ruzene, C., Schmer, B., Sinha, B., Day, D. A., Andreae, M. O., Jimenez, J. L., Gallagher, M., Kreidenweis, S. M., Bertram, A. K., and Pöschl, U.: High concentrations of biological aerosol par- ticles and ice nuclei during and after rain, Atmos. Chem. Phys., 13, 6151–6164, doi:10.5194/acp-13-6151-2013, 2013

Ijaz, A., Temime-Roussel, B., Chazeau, B., Albertin, S., Arnold, S. R., Barrett, B., Bekki, S., Brett, N., Cesler-Maloney, M., Dieudonne, E., Dingilian, K. K., Fochesatto, J. G., Mao, J., Moon, A., Savarino, J., Simpson, W., Weber, R. J., Law, K. S., & D'Anna, B. (2024). Complementary Aerosol Mass Spectrometry Elucidates Sources of Wintertime Sub-Micron Particle Pollution in Fairbanks, Alaska, during Alpaca 2022 . https://doi.org/10.5194/egusphere-2024-3789

Kieft, T. L. (1988). Ice nucleation activity in lichens. Applied and Environmental Microbiology, 54(7), 1678–1681. https://doi.org/10.1128/aem.54.7.1678-1681.1988

Lill, E., Costa, E. J., Barry, K., Mirrielees, J. A., Mashkevich, M., Wu, J., Holen, A. L., Cesler-Maloney, M., DeMott, P. J., Perkins, R., Hill, T., Sullivan, A., Levin, E., Simpson, W. R., Mao, J., Temime-Roussel, B., D'Anna, B., Law, K. S., Ault, A. P., … Creamean, J. (2024). The abundance and sources of ice nucleating particles within Alaskan ice fog. *Journal of Geophysical Research: Atmospheres*, e2024JD041170. https://doi.org/10.1029/2024JD041170

Macander, M. J., Palm, E. C., Frost, G. V., Herriges, J. D., Nelson, P. R., Roland, C., Russell, K. L., Suitor, M. J., Bentzen, T. W., Joly, K., Goetz, S. J., & Hebblewhite, M. (2020). Lichen cover mapping for Caribou Ranges in interior Alaska and Yukon. Environmental Research Letters, 15(5), 055001. https://doi.org/10.1088/1748-9326/ab6d38

Maki, L. R., Galyan, E. L., Chang-Chien, M.-M., & Caldwell, D. R. (1974). Ice nucleation induced by pseudomonas syringae. Applied Microbiology, 28(3), 456–459. https://doi.org/10.1128/am.28.3.456-459.1974

Malingowski, J., Atkinson, D., Fochesatto, J., Cherry, J., & Stevens, E. (2014). An observational study of radiation temperature inversions in Fairbanks, Alaska. Polar Science, 8(1), 24–39. https://doi.org/10.1016/j.polar.2014.01.002

Mason, R. H., Si, M., Chou, C., Irish, V. E., Dickie, R., Elizondo, P., Wong, R., Brintnell, M., Elsasser, M., Lassar, W. M., Pierce, K. M., Leaitch, W. R., MacDonald, A. M., Platt, A., Toom-Sauntry, D., Sarda-Estève, R., Schiller, C. L., Suski, K. J., Hill, T. C. J., … Bertram, A. K. (2016). Size-resolved measurements of ice-nucleating particles at six locations in North America and one in Europe. *Atmospheric Chemistry and Physics*, 16, 1637–1651. https://doi.org/10.5194/acp-16-1637-2016

McCluskey, C. S., Hill, T. C., Humphries, R. S., Rauker, A. M., Moreau, S., Strutton, P. G., Chambers, S. D., Williams, A. G., McRobert, I., Ward, J., Keywood, M. D., Harnwell, J., Ponsonby, W., Loh, Z. M., Krummel, P. B., Protat, A., Kreidenweis, S. M., & DeMott, P. J. (2018). Observations of ice nucleating particles over Southern Ocean waters. Geophysical Research Letters, 45(21). https://doi.org/10.1029/2018gl079981

Moon, A., Jongebloed, U., Dingilian, K. K., Schauer, A. J., Chan, Y.-C., Cesler-Maloney, M., Simpson, W. R., Weber, R. J., Tsiang, L., Yazbeck, F., Zhai, S., Wedum, A., Turner, A. J., Albertin, S., Bekki, S., Savarino, J., Gribanov, K., Pratt, K. A., Costa, E. J., … Alexander, B. (2023). Primary sulfate is the dominant source of particulate sulfate during winter in Fairbanks, Alaska. ACS ES&T Air, 1(3), 139–149. https://doi.org/10.1021/acsestair.3c00023

Nicholls, D. L., Brackley, A. M., & Barber, V.(2010). *Wood energy for residential heating in Alaska: Current conditions, attitudes, and expected use. Gen. Tech. Rep. PNW-GTR-826*(Vol. **30**). U.S. Department of Agriculture, Forest Service, Pacific Northwest Research Station. 826. https://doi.org/10.2737/PNW-GTR-826

O'Sullivan, D., Adams, M. P., Tarn, M. D., Harrison, A. D., Vergara-Temprado, J., Porter, G. C. E., et al. (2018). Contributions of biogenic material to the atmospheric ice-nucleating particle

population in North Western Europe. *Scientific Reports*, **8**(1), 13821. https://doi.org/10.1038/s41598-018-31981-7

Pruppacher, H. R., & Klett, J. D. (1997). *Microphysics of cloud and precipitation*. Kluwer Academic Publishers.

Petters, M. D., Parsons, M. T., Prenni, A. J., DeMott, P. J., Kreidenweis, S. M., Carrico, C. M., et al. (2009). Ice nuclei emissions from biomass burning. Journal of Geophysical Research, 114(D7), D07209. https://doi.org/10.1029/2008JD011532

Petters, M. D., et al., Ice nuclei emissions from biomass burning, Journal of Geophysical Research, doi:10.10292008JD011532, 2015.

Rogers, D. C., P. J. DeMott, S. M. Kreidenweis, and Y. Chen, 2001: A Continuous-Flow Diffusion Chamber for Airborne Measurements of Ice Nuclei. J. Atmos. Oceanic Technol., 18, 725–741, https://doi.org/10.1175/1520-0426(2001)018<0725:ACFDCF>2.0.CO;2.

Rosinski, J., Haagenson, P. L., Nagamoto, C. T., and Parungo, F.: Ice-forming nuclei of maritime origin, J. Aerosol Sci., 17, 23– 46, doi:10.1016/0021-8502(86)90004-2, 1986

Rucklidge, J. (1965). The examination by electron microscope of ice crystal nuclei from Cloud Chamber experiments. Journal of the Atmospheric Sciences, 22(3), 301–308. https://doi.org/10.1175/1520-0469(1965)022<0301:tebemo>2.0.co;2

Schill, G. P., Jathar, S. H., Kodros, J. K., Levin, E. J., Galang, A. M., Friedman, B., Link, M. F., Farmer, D. K., Pierce, J. R., Kreidenweis, S. M., & DeMott, P. J. (2016). Ice-nucleating particle emissions from photochemically aged diesel and biodiesel exhaust. Geophysical Research Letters, 43(10), 5524–5531. https://doi.org/10.1002/2016gl069529

Schmitt, C. G., Stuefer, M., Heymsfield, A. J., & Kim, C. K. (2013). The microphysical properties of ice fog measured in urban environments of Interior Alaska. *Journal of Geophysical Research: Atmospheres*, **118**(19), 11136–11147. https://doi.org/10.1002/jgrd.50822

Schmale, J., Arnold, S. R., Law, K. S., Thorp, T., Anenberg, S., Simpson, W. R., et al. (2018). Local Arctic air pollution: A neglected but serious problem. *Earth's Future*, **6**(10), 1385–1412. https://doi.org/10.1029/2018EF000952
Schwarz, J. P., Gao, R. S., Perring, A. E., Spackman, J. R. and Fa- hey, D. W.: Black carbon aerosol size in snow, Sci. Rep., 3, 1356, doi:10.1038/srep01356, 2013.

Schwarz, J. P., Gao, R. S., Spackman, J. R., Watts, L. A., Thomson, D. S., Fahey, D. W., Ryerson, T. B., Peischl, J., Holloway, J. S., Trainer, M., Frost, G. J., Baynard, T., Lack, D. A., de Gouw, J. A., Warneke, C., and Del Negro, L. A.: Measurement of the mixing state, mass, and optical size of individual black carbon particles in urban and biomass burning emissions, Geophys. Res. Lett., 35, L13810, doi:10.1029/2008GL033968, 2008.

Sesartic, A. and Dallafior, T. N.: Global fungal spore emissions, re- view and synthesis of literature data, Biogeosciences, 8, 1181– 1192, doi:10.5194/bg-8-1181-2011, 2011.

Shi, Y., Creamean, J., Hill, T., Hume, C., & Vazquez, M. Ice Nucleation Spectrometer for INP measurement (INP), 2022-06-04 to 2022-09-29, ARM Mobile Facility (HOU), Houston, TX; AMF1 (main site for TRACER) (M1). Atmospheric Radiation Measurement (ARM) User Facility. https://doi.org/10.5439/1770816

Suski, K. J., Hill, T. C. J., Levin, E. J. T., Miller, A., DeMott, P. J., & Kreidenweis, S. M. (2018). Agricultural harvesting emissions of ice-nucleating particles. *Atmospheric Chemistry and Physics*, **18**(18), 13755–13771. https://doi.org/10.5194/acp-18-13755-2018

Testa, B., Hill, T. C., Marsden, N. A., Barry, K. R., Hume, C. C., Bian, Q., Uetake, J., Hare, H., Perkins, R. J., Möhler, O., Kreidenweis, S. M., & DeMott, P. J. (2021). Ice nucleating particle connections to regional Argentinian land surface emissions and weather during the cloud, aerosol, and complex Terrain Interactions Experiment. Journal of Geophysical Research: Atmospheres, 126(23). https://doi.org/10.1029/2021jd035186

Tian, P., Liu, D., Bi, K., Huang, M., Wu, Y., Hu, K., Li, R., He, H., Ding, D., Hu, Y., Liu, Q., Zhao, D., Qiu, Y., Kong, S., & Xue, H. (2022). Evidence for anthropogenic organic aerosols contributing to ice nucleation. *Geophysical Research Letters*, 49(16), e2022GL099990. https://doi.org/10.1029/2022GL099990

Tobo, Y., Uetake, J., Matsui, H., Moteki, N., Uji, Y., Iwamoto, Y., Miura, K., & Misumi, R. (2020). Seasonal trends of atmospheric ice nucleating particles over Tokyo. *Journal of Geophysical Research: Atmospheres*, 125(22), e2020JD033658. https://doi.org/10.1029/2020JD033658

Tran, H. N. Q., & Mölders, N. (2011). Investigations on meteorological conditions for elevated PM2.5 in Fairbanks, Alaska. *Atmospheric Research*, **99**(1), 39–49. https://doi.org/10.1016/j.atmosres.2010.08.028

Trebs, I., Lett, C., Krein, A., Matsumoto Kawaguchi, E., & Junk, J. (2024). Performance evaluation of an online monitor based on X-ray fluorescence for detecting elemental concentrations in ambient particulate matter. *Atmospheric Measurement Techniques*, 17, 6791–6806. https://doi.org/10.5194/amt-17-6791-2024

Wagh, S., Singh, P., Ghude, S. D., Safai, P., Prabhakaran, T., & Kumar, P. P. (2021). Study of ice nucleating particles in fog-haze weather at New Delhi, India: A case of polluted environment. *Atmospheric Research*, 258, 105693. https://doi.org/10.1016/j.atmosres.2021.105693

Vali, G. 1971. “Quantitative Evaluation of Experimental Results and the Heterogeneous Freezing Nucleation of Supercooled Liquids.” Journal of the Atmospheric Sciences 28(3): 402–409, https://doi.org/10.1175/1520-0469(1971)028<0402:QEOERA>2.0.CO;2

Wang, Y.; Hopke, P. K. Is Alaska Truly the Great Escape from Air Pollution? - Long Term Source Apportionment of Fine Particulate Matter in Fairbanks, Alaska. *Aerosol Air Qual. Res.* **2014**, *14* (7), 1875– 1882, DOI: 10.4209/aaqr.2014.03.0047

Ward, T.; Trost, B.; Conner, J.; Flanagan, J.; Jayanty, R. K. M. Source Apportionment of PM2.5 in a Subarctic Airshed - Fairbanks, Alaska. *Aerosol Air Qual. Res.* **2012**, *12*, 536– 543, DOI: 10.4209/aaqr.2011.11.0208

Wendler, G., & Jayaweera, K. O. L. F. (1972). Some measurements of the development of the surface inversion in Central Alaska during winter. *Pure and Applied Geophysics*, **99**(1), 209–221. https://doi.org/10.1007/BF00875277

Wex, H., Huang, L., Zhang, W., Hung, H., Traversi, R., Becagli, S., Sheesley, R. J., Moffett, C. E., Barrett, T. E., Bossi, R., Skov, H., Hünerbein, A., Lubitz, J., Löffler, M., Linke, O., Hartmann, M., Herenz, P., & Stratmann, F. (2019). Annual variability of ice-nucleating particle concentrations at different Arctic locations. Atmospheric Chemistry and Physics, 19(7), 5293–5311. https://doi.org/10.5194/acp-19-5293-2019

Willis, R. A., & Grice, G. K. (1977). The wintertime Arctic front and its effect on Fairbanks, Alaska. *Monthly Weather Review*, **105**(1), 78–85. https://doi.org/10.1175/1520-0493(1977)105<0078:TWAFAI>2.0.CO;2

Ye, L.; Wang, Y. Long-Term Air Quality Study in Fairbanks, Alaska: Air Pollutant Temporal Variations, Correlations, and PM2.5 Source Apportionment. *Atmosphere* **2020**, *11* (11), 1203, DOI: 10.3390/atmos11111203